



**Nimodipine reduces microglial activation in vitro as evidenced by morphological phenotype, phagocytic activity and high-throughput RNA sequencing**

Journal:	<i>British Journal of Pharmacology</i>
Manuscript ID	2024-BJP-1452-RP.R2
Manuscript Type:	Research Article
Date Submitted by the Author:	n/a
Complete List of Authors:	<p>Pesti, István; Hungarian Centre of Excellence for Molecular Medicine, HCEMM-USZ Cerebral Blood Flow and Metabolism Research Group; University of Szeged, Department of Cell Biology and Molecular Medicine</p> <p>Varga, Valentin; Delta Bio 2000 Ltd., 6726 Szeged, Hungary</p> <p>Qorri, Erda; Delta Bio 2000 Ltd., 6726 Szeged, Hungary</p> <p>Frank, Rita; Hungarian Centre of Excellence for Molecular Medicine, HCEMM-USZ Cerebral Blood Flow and Metabolism Research Group; University of Szeged, Department of Cell Biology and Molecular Medicine</p> <p>Kata, Diána; University of Szeged, Institute of Laboratory Medicine</p> <p>Vinga, Krisztián; University of Szeged, Department of Cell Biology and Molecular Medicine</p> <p>Szarvas, Péter; Hungarian Centre of Excellence for Molecular Medicine, HCEMM-USZ Cerebral Blood Flow and Metabolism Research Group; University of Szeged, Department of Cell Biology and Molecular Medicine</p> <p>Menyhárt, Ákos; Hungarian Centre of Excellence for Molecular Medicine, HCEMM-USZ Cerebral Blood Flow and Metabolism Research Group; University of Szeged, Department of Cell Biology and Molecular Medicine</p> <p>Gulya, Karoly; University of Szeged, Department of Cell Biology and Molecular Medicine</p> <p>Bari, Ferenc; University of Szeged, Department of Medical Physics and Informatics</p> <p>Farkas, Eszter; Hungarian Centre of Excellence for Molecular Medicine, HCEMM-USZ Cerebral Blood Flow and Metabolism Research Group; University of Szeged, Department of Cell Biology and Molecular Medicine</p>
Major area of pharmacology:	Neuropharmacology, Neurodegeneration/neuroprotection
Cross-cutting area:	Pharmacogenomics/pharmacogenetics, Inflammation
Additional area(s):	Ion channels, Repurposing

SCHOLARONE™  
Manuscripts

1  
2  
3  
4  
5  
6  
7  
8  
9  
10  
11  
12  
13  
14  
15  
16  
17  
18  
19  
20  
21  
22  
23  
24  
25  
26  
27  
28  
29  
30  
31  
32  
33  
34  
35  
36  
37  
38  
39  
40  
41  
42  
43  
44  
45  
46  
47  
48  
49  
50  
51  
52  
53  
54  
55  
56  
57  
58  
59  
60



UNIVERSITAS SCIENTIARUM SZEGEDIENSIS  
UNIVERSITY OF SZEGED

Albert Szent-Györgyi Medical School, Faculty of Science and Informatics  
Department of Cell Biology and Molecular Medicine

P. Ferdinandy, PhD  
Semmelweis University, Budapest, Hungary  
Editor-in-Chief  
British Journal of Pharmacology

Date: Szeged, March 13, 2025

Topic: Manuscript revision

Dear Dr. Ferdinandy,

Please, find enclosed a revised manuscript titled ***“Nimodipine reduces microglial activation in vitro as evidenced by morphological phenotype, phagocytic activity and high-throughput RNA sequencing”*** by István Pesti et al., submitted as an original Research Article to the British Journal of Pharmacology.

We thank the Editors and the Reviewers for their supportive opinion on the revised submission. In our best effort to comply with the remaining suggestion of Reviewer #1, a relevant addition has been made to the Discussion section to improve and refine the interpretation of the data. The changes to the manuscript within the document have been highlighted by using coloured text (red font). Please note that the addition increased the word count of the paper by 165 words, with 6 additional entries in the reference list.

In recent years, there has been a surge of interest in drug repurposing, which has been estimated to halve valuable drug-to-the-market time and curb costs significantly, by relying on existing safety and toxicology data and by the reduced need for safety trials. Here, we explore a new application for nimodipine, a vasodilator used to prevent delayed ischemic deficit in patients with aneurysmal subarachnoid hemorrhage. We present experimental data showing that nimodipine directly inhibits microglial activation typical of acute brain injury. We believe that the research presented in the manuscript falls within the scope of the British Journal of Pharmacology. Microglial activation is the focus of the paper as a potential target for neuroprotection in brain injury. The impact of nimodipine on microglial activation was evaluated here by determining morphological and functional phenotypic states, along with the analysis of microglial transcriptomic profiles. We have identified that the expression of 110 genes was altered by nimodipine to oppose microglial activation, of which at least one fifth was associated with microglial immune response, several with cell adhesion and some with autophagy regulation. We are confident that these findings, collected in live brain slice preparations and primary microglial co-cultures and monocultures, will contribute significantly to the renewed general interest in nimodipine.



UNIVERSITAS SCIENTIARUM SZEGEDIENSIS  
**UNIVERSITY OF SZEGED**

Albert Szent-Györgyi Medical School, Faculty of Science and Informatics  
**Department of Cell Biology and Molecular Medicine**

All authors have contributed to the manuscript significantly and have approved the final version of the paper. The manuscript has not been published elsewhere, in full or in part, nor is it under consideration by another publisher. The manuscript has been uploaded to the preprint server bioRxiv with the reference number BIORXIV/2024/623031. No generative artificial intelligence was used for data analysis or manuscript preparation. We disclose no financial or other relationships that might lead to a perceived conflict of interest.

We hope that the Editors and the Reviewers find merit in our work, find our responses adequate and acceptable, and support the publication of the paper.

On behalf of all the authors,  
Yours sincerely,

A handwritten signature in blue ink, appearing to read 'Eszter Farkas'.

Eszter Farkas, Ph.D., D.Sc.  
Corresponding Author

HCEMM-USZ Cerebral Blood Flow and Metabolism  
Research Group  
Department of Cell Biology and Molecular Medicine  
Albert Szent-Györgyi Medical School, Faculty of  
Science and Informatics, University of Szeged  
Somogyi u. 4, H-6720 Szeged, Hungary  
E-mail: farkas.eszter.1@med.u-szeged.hu

## RESPONSE TO THE EDITORS' AND REVIEWERS' SUGGESTIONS

**Submission ID:** 2024-BJP-1452-RP-R2

**Title:** Nimodipine reduces microglial activation in vitro as evidenced by morphological phenotype, phagocytic activity and high-throughput RNA sequencing

**Authors:** István Pesti, Valentin Varga, Erda Qorri, Rita Frank, Diana Kata, Krisztián Vinga, Péter Archibald Szarvas, Ákos Menyhárt, Károly Gulya, Ferenc Bari, Eszter Farkas

We thank the Editors and the Reviewers for their supportive opinion on the revised submission. In our best effort to comply with the remaining suggestion of Reviewer #1, a relevant addition has been made to the Discussion section to improve and refine the interpretation of the data.

The changes to the manuscript within the document have been highlighted by using coloured text (red font). To expedite the processing of the manuscript, we provide our response to the comment of Reviewer #1 below. Please note that the addition increased the word count of the paper by 165 words, with 6 additional entries in the reference list.

We hope that the Editors and the Reviewers find merit in our work, find our response adequate and acceptable, and support the publication of the paper.

### REVIEWERS' COMMENTS TO AUTHOR

#### Reviewer #1

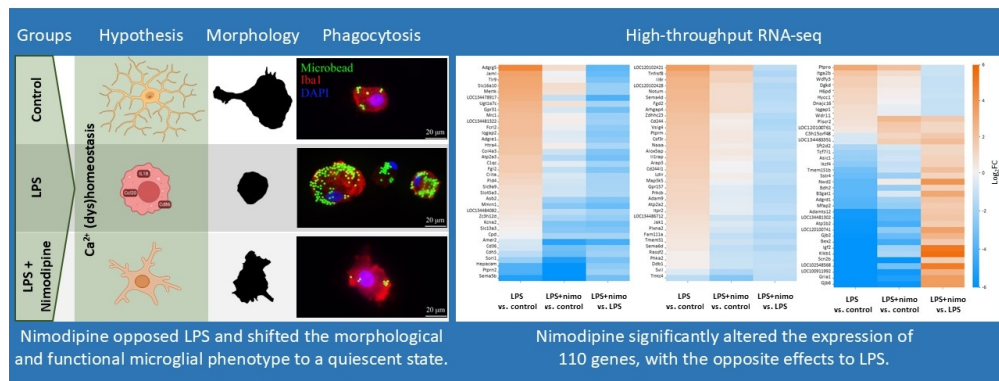
**Q1:** The authors have addressed most of my concerns but should add the dose considerations to the discussion. It will be important for the average reader to understand that in order to reduce neuroinflammation in a clinical setting, nimodipine needs to be dosed an order of magnitude higher. That should not just "be brushed under the carpet".

**Re:** Thank you for pointing out the need to include our arguments in the manuscript – we did not intend to conceal this issue. The Discussion has been updated to include a paragraph on nimodipine concentration.

#### Reviewer #2

no comments

# Nimodipine suppresses microglial activation



Pesti, et al. *Br. J. Pharmacol.*



338x190mm (96 x 96 DPI)

**BULLET POINT SUMMARY**

Pest et al.,

Nimodipine reduces microglial activation *in vitro* as evidenced by morphological phenotype, phagocytic activity and next generation RNA sequencing

**What is already known**

- Nimodipine is an approved L-type voltage-gated calcium channel blocker.
- Nimodipine is in clinical use to prevent delayed ischemic deficit following subarachnoid hemorrhage.

**What this study adds**

- Nimodipine suppressed the amoeboid morphological transformation and phagocytosis of activated microglia.
- Nimodipine altered the expression of 110 genes concerning immune response, cell adhesion and autophagy regulation .

**Clinical significance**

- Nimodipine is suggested to attenuate neuroinflammation in acute brain injury or chronic neurodegeneration.
- The medical field of indication of nimodipine should be expanded.

1  
2  
3 **Nimodipine reduces microglial activation *in vitro* as evidenced by morphological phenotype, phagocytic**  
4 **activity and high-throughput RNA sequencing**  
5  
6  
7

8 István Pesti<sup>1,2</sup>, Valentin Varga<sup>3</sup>, Erda Qorri<sup>3</sup>, Rita Frank<sup>1,2</sup>, Diana Kata<sup>4</sup>, Krisztián Vinga<sup>2</sup>, Péter Archibald  
9 Szarvas<sup>1,2</sup>, Ákos Menyhárt<sup>1,2</sup>, Károly Gulya<sup>2</sup>, Ferenc Bari<sup>5</sup>, Eszter Farkas<sup>1,2\*</sup>  
10  
11

12  
13 <sup>1</sup>Hungarian Centre of Excellence for Molecular Medicine – University of Szeged Cerebral Blood Flow and  
14 Metabolism Research Group, Szeged, Hungary; Somogyi u 4, 6720 Szeged, Hungary;

15  
16 <sup>2</sup>Department of Cell Biology and Molecular Medicine, Albert Szent-Györgyi Medical School and Faculty of  
17 Science and Informatics, University of Szeged; Szeged, Hungary; Somogyi u 4, 6720 Szeged, Hungary  
18

19  
20 <sup>3</sup>Delta Bio 2000 Ltd., 6726 Szeged, Hungary

21  
22 <sup>4</sup>Institute of Laboratory Medicine, University of Szeged, Szeged, Hungary

23  
24 <sup>5</sup>Department of Medical Physics and Informatics, Albert Szent-Györgyi Medical School and Faculty of Science  
25 and Informatics, University of Szeged; Szeged, Hungary; Korányi fasor 9, 6720 Szeged, Hungary  
26  
27  
28  
29  
30  
31  
32

33 **\*Correspondence**

34 Eszter Farkas, D.Sc. (ORCID: 0000-0002-8478-9664)

35 HCEMM-USZ Cerebral Blood Flow and Metabolism Research Group

36 Department of Cell Biology and Molecular Medicine

37 Szent-Györgyi Albert Medical School

38 Faculty of Science and Informatics

39 University of Szeged

40 Somogyi u. 4

41 H-6720 Szeged

42 Hungary

43 Tel.: +36 62 342 208

44 E-mail: [farkas.eszter.1@med.u-szeged.hu](mailto:farkas.eszter.1@med.u-szeged.hu)  
45  
46  
47  
48  
49  
50  
51  
52  
53  
54  
55  
56  
57  
58  
59  
60

## Abstract

**Background and Purpose** Nimodipine, an L-type voltage-gated calcium channel blocker, is an approved cerebral vasorelaxant. We hypothesize that nimodipine attenuates the pro-inflammatory shift in microglial phenotype. Here we analysed the effects of nimodipine on morphological and functional microglial phenotypes as well as their transcriptomic profile.

**Experimental Approach** Live brain slice preparations from C57BL/6 mice and primary microglia cultures from neonatal Sprague Dawley rats were used. Microglia were activated by ischemia or lipopolysaccharide (LPS), and preparations were treated with nimodipine (5-10-20  $\mu$ M). Microglial morphological phenotype, phagocytic activity, Iba1 expression and TNF $\alpha$  levels were evaluated. Total RNA was isolated from monocultures and processed for next generation RNA sequencing.

**Key Results** LPS resulted in a pro-inflammatory microglial phenotype, affecting the expression of cytokines, the complement system and phagocytosis-related genes. LPS increased the transcription of ionotropic purinergic and some TRP channels but decreased the expression of voltage- and ligand-gated calcium channels, downregulated the expression of Ryr and IP3 receptors and increased transcription of the SERCA calcium pump. Nimodipine suppressed the amoeboid morphological transformation and phagocytosis and altered the expression of 110 genes in the opposite direction to LPS activation, of which at least 20 were associated with microglial immune response, 7 with cell adhesion and 2 with autophagy regulation.

**Conclusion and Implications** The effect of nimodipine goes beyond cerebral vasorelaxation. Nimodipine attenuates microglial activation by modulating Ca<sup>2+</sup>-dependent gene expression involved in intracellular signalling cascades to drive microglial immune responses. Consideration should be given to expanding the medical field of indication of nimodipine.

## Keywords

Calcium channel, Microglia, Neuroinflammation, Nimodipine, Phagocytosis, Transcriptomics, Voltage-gated calcium channel

**List of abbreviations**

aCSF,	artificial cerebrospinal fluid
AMPA,	$\alpha$ -amino-3-hydroxy-5-methyl-4-isoxazole-propionic acid
ANOVA,	one-way analysis of variance
BP,	biological processes
CFTR,	cystic fibrosis transmembrane conductance regulator
CRAC	Ca <sup>2+</sup> release-activated Ca <sup>2+</sup> channel
DEG,	differentially expressed gene
ER,	endoplasmic reticulum
GO,	gene ontology
Iba1,	ionized calcium binding adaptor molecule 1
IFN $\gamma$ ,	interferon- $\gamma$
IL-10,	interleukin-10
IL-1 $\beta$ ,	interleukin-1 $\beta$
IP3R,	inositol triphosphate receptor
LPS,	lipopolysaccharide
LVGCC,	L-type voltage gated calcium channel
NMDA,	N-methyl-D-aspartate
mOGD,	mild oxygen-glucose deprivation
PCA,	principal component analysis
PGE <sub>2</sub> ,	prostaglandin E <sub>2</sub>
RANTES,	regulated on activation, normal T-cell expressed and secreted
RNA-Seq,	RNA-sequencing
Ryr,	ryanodine receptor
SD,	spreading depolarization
stdev,	standard deviation
SERCA,	sarcoplasmic/endoplasmic reticulum Ca <sup>2+</sup> -ATPase
TI,	transformation index
TLR4,	toll-like receptor 4
TNF- $\alpha$ ,	tumor necrosis factor- $\alpha$
TPM,	transcripts per million
TRP,	transient receptor potential
VGCC,	voltage gated calcium channel

## Introduction

Nimodipine is a 1,4-dihydropyridine L-type voltage-gated calcium channel (LVGCC) blocker (Tang et al., 2016). The primary targets of nimodipine are cerebrovascular smooth muscle cells (Kazda and Towart, 1982). Nimodipine achieves vasorelaxation by inhibiting  $\text{Ca}^{2+}$  influx through LVGCCs, thereby reducing  $\text{Ca}^{2+}$ -dependent activation of smooth muscle cell contractile activity. Nimodipine has clinical therapeutic value in the prevention of delayed ischemic deficit following subarachnoid haemorrhage (Allen et al., 1983; Feigin et al., 1998). In addition, recent preclinical investigations have revisited the possibility that nimodipine may provide therapeutic benefit in selected patients with ischemic stroke or migraine with aura (Carlson et al., 2020), and have experimentally shown that a common pathomechanism known as spreading depolarization (SD) can be partially inhibited by nimodipine (Dietz, Weiss et al., 2008; Frank et al., 2024; Menyhárt et al., 2018 & 2024; Szabó et al., 2019).

In addition to vascular smooth muscle cells, LVGCCs are expressed in various cell types of the nervous tissue, including microglia (Colton et al., 1994; Espinosa-Parrilla et al., 2015). Microglia are the resident immune cells in the central nervous system, which become rapidly activated by exogenous pathogens or endogenous danger signals upon brain injury. Activated microglia can assume functional states that are implicated in neuroinflammation and neurotoxicity. Importantly, microglial activation has been associated with altered intracellular  $\text{Ca}^{2+}$  homeostasis (Hopp et al., 2020). *In vivo* two-photon imaging identified distinct microglial  $\text{Ca}^{2+}$  transients in response to acute neuronal injury (Eichhoff et al., 2011) and prominent microglial  $\text{Ca}^{2+}$  waves associated with SD in experimental ischemic stroke (Liu et al., 2021). Exposure of cultured microglia to the bacterial lipopolysaccharide (LPS) revealed a sustained  $\text{Ca}^{2+}$  load of the cells, which blunted receptor-mediated  $\text{Ca}^{2+}$  transients (Hoffmann et al., 2003). Part of the  $\text{Ca}^{2+}$  influx upon microglial activation must be mediated by LVGCCs. For example, various LVGCC blockers reduced the intracellular  $\text{Ca}^{2+}$  load in microglia activated with prion protein or beta-amyloid fragments (Silei et al., 1999), and the addition of nimodipine attenuated RANTES (a pro-inflammatory chemokine)-induced  $\text{Ca}^{2+}$  accumulation in cultured microglia (Hegg et al., 2000). Further, a  $\text{Ca}^{2+}$  current via LVGCCs sensitive to nifedipine (a dihydropyridine calcium channel blocker similar to nimodipine) was associated with superoxide production by microglia (Colton et al., 1994). Finally, nimodipine administered to LPS-activated microglial cultures inhibited the production of the pro-inflammatory tumor necrosis factor- $\alpha$  (TNF- $\alpha$ ), interleukin-1 $\beta$  (IL-1 $\beta$ ) and prostaglandin  $\text{E}_2$  (PGE $_2$ ) (Li et al., 2009). The effect of nimodipine on microglial LVGCCs is logical because microglia express the Cav1.2 and Cav1.3 isoforms of the pore-forming  $\alpha$  subunit of the channel (Espinosa-Parrilla et al., 2015; Hopp et al., 2020), for which nimodipine affinity has been described (Huang et al., 2013; Xu and Lipscombe, 2001). It remains to be determined, which intracellular signalling cascades link the pro-inflammatory shift in microglial phenotype to intracellular  $\text{Ca}^{2+}$  oscillations.

1  
2  
3 We have recently found that nimodipine given to the bath of metabolically challenged (mild oxygen-  
4 glucose deprivation) live brain slice preparations undergoing SD shifts the morphological phenotype of  
5 activated microglia to a more quiescent state, as evidenced by richer microglial ramifications (Frank et al.,  
6 2024). However, the model system does not allow to separate direct nimodipine effects on microglia from  
7 indirect actions (e.g. nimodipine altering neuronal excitation to which microglia respond), because LVGCCs are  
8 ubiquitously expressed in several cell types in the brain tissue, including neurons, astrocytes, and  
9 oligodendrocytes (Hopp et al., 2020). Primary microglial cultures have been used to study microglial activation  
10 and the effect of different pharmacological agents on microglial states selectively (Pesti et al., 2024). Further,  
11 transcriptomic analysis of cultured microglia activated with LPS revealed the induction of pro-inflammatory  
12 genes, interferon-induced genes, and immune activation genes (Pulido-Salgado et al., 2018; Sabogal-Guáqueta  
13 et al., 2023). Building on these insights, the objective of this study was to comprehensively analyse the effects  
14 of nimodipine on activated microglia at the level of morphological and functional phenotypes, as well as their  
15 transcriptomic profile. We sought to identify Ca<sup>2+</sup> dependent signalling cascades through which nimodipine  
16 may attenuate the pro-inflammatory shift in microglial function. The collected evidence suggests that  
17 nimodipine exerts distinct anti-inflammatory potential, which could be considered when expanding the field  
18 of clinical indication of nimodipine.  
19  
20  
21  
22  
23  
24  
25  
26  
27  
28  
29  
30

## 31 **Materials and Methods**

### 32 *Ethics declaration*

33  
34  
35  
36  
37  
38 Animal studies are reported in compliance with the ARRIVE guidelines (Kilkenny et al., 2010) and with the  
39 recommendations made by the British Journal of Pharmacology. Experimental procedures were approved by  
40 the National Food Chain Safety and Animal Health Directorate of Csongrád-Csanád County, Hungary  
41 (II./1131/2018 and XXXII./4050/2020). The experiments were performed according to the guidelines of the  
42 Scientific Committee of Animal Experimentation of the Hungarian Academy of Sciences, following the EU  
43 Directive 2010/63/EU.  
44  
45  
46  
47

48 For live brain slice preparations, adult, C57BL/6 mice from both sexes (body weight: 18-24 g; n=15) were  
49 used in this study. Animals (Charles River Laboratories breed) were acquired from the Central Animal House  
50 of Biological Research Center, Szeged, Hungary. Standard rodent chow and tap water were supplied *ad libitum*.  
51 The animals were housed under constant temperature, humidity, and lighting conditions (23 °C, 12:12 h light/  
52 dark cycle, lights on at 6 a.m.). For microglial cell cultures, pregnant Sprague-Dawley rats (170-190 g; one  
53 animal per cage) were maintained under standard housing conditions and fed *ad libitum*. Five breeding runs  
54 (4-6 pregnant rats each) provided the litters (6-12 pups from each mother) from which independent culture  
55 experiments were performed.  
56  
57  
58  
59  
60

### *Brain slice preparations*

Coronal brain slices were prepared as previously reported (Frank et al., 2024). Briefly, C57BL/6 mice (male and female randomly selected) were deeply anesthetized with 5% isoflurane (in N<sub>2</sub>O:O<sub>2</sub>; 2:1), the animals were decapitated, 350 µm thick coronal brain slices were cut anterior to the bregma using a vibrating blade microtome (Leica VT1000S, Leica, Germany) and collected in ice-cold cutting aCSF (130 NaCl, 3.5 KCl, 1 NaH<sub>2</sub>PO<sub>4</sub>, 24 NaHCO<sub>3</sub>, 1 CaCl<sub>2</sub>, 3 MgSO<sub>4</sub>, and 10 d-glucose in mM concentrations). After cutting, three to five slices were allowed to recover in carbogenated normal aCSF (130 NaCl, 3.5 KCl, 1 NaH<sub>2</sub>PO<sub>4</sub>, 24 NaHCO<sub>3</sub>, 3 CaCl<sub>2</sub>, 1.5 MgSO<sub>4</sub>, and 10 d-glucose in mM concentrations) for 30 min. Randomly selected slices were placed in an interface-type tissue chamber (Brain Slice Chamber BSC1, Scientific Systems Design Inc., Ontario, Canada) and continuously perfused with carbogenated aCSF at a rate of 2.5 ml/min. Chamber temperature was maintained at 32°C using a dedicated proportional temperature control unit (PTC03, Scientific Systems Design Inc., Ontario, Canada). Microglia in brain slice preparations were activated by mild oxygen-glucose deprivation (mOGD), achieved by superfusion of aCSF containing 5 mM D-glucose (reduced to 50%) for 45 min and transient hypoxia which was induced by the withdrawal of carbogen for 60 seconds three times at 15-minute intervals (Frank et al., 2024). Hypoxic episodes gave rise to SD (Frank et al., 2024). Brain slices were randomly assigned to a nimodipine-treated or a control group. The slices were bathed in nimodipine-enriched aCSF (10 µM final nimodipine concentration) for 30 min before and 45 min during mOGD, prior to histological processing.

### *Maintenance and treatment of cell cultures*

Primary cortical cell co-cultures were isolated from newborn rats, and microglial monocultures were derived from the co-cultures as previously described (Szabo and Gulya, 2013). Briefly, cerebrocortical tissue from male and female newborn Sprague-Dawley rat pups (P1) was rapidly dissected, pooled, minced, and dissociated in 0.25% trypsin for 10 min at 37°C. The trypsin was then neutralized with Dulbecco's modified Eagle's medium (DMEM) containing 1 g/L D-glucose, 110 mg/mL Na-pyruvate, 4 mM L-glutamine, 3.7 g/L NaHCO<sub>3</sub>, 10,000 U/mL penicillin G, 10 mg/mL streptomycin sulphate, and 25 µg/mL amphotericin B and 15% heat-inactivated foetal bovine serum (FBS; Thermo Fisher Scientific, Carlsbad, CA, USA). After centrifugation at 1000g for 10 minutes at room temperature (RT), the pellet was resuspended, washed in 10 mL DMEM containing 10% FBS, and centrifuged again at 1000g and RT for 10 minutes. The final pellet was filtered through a sterile filter (100 µm pore size; Greiner Bio-One Hungary Kft., Mosonmagyaróvár, Hungary) to remove tissue fragments that had resisted dissociation. The cells were resuspended in 2 mL of the same solution and then seeded on poly-L-lysine-coated culture flasks (75 cm<sup>2</sup>; 10<sup>7</sup> cells/flask) or poly-L-lysine-coated coverslips (15×15 mm; 2×10<sup>5</sup> cells/coverslip) for immunocytochemistry or in poly-L-lysine-coated Petri dishes (60 mm × 15 mm;

1  
2  
3 10<sup>6</sup> cells/Petri dish) for Western blot analysis and cultured at 37°C in a humidified air atmosphere  
4 supplemented with 5% CO<sub>2</sub>. The medium was changed the next day and every 3 days thereafter. After 7 days  
5 of culture, microglial cells in primary co-cultures (DIV7) were shaken on a platform shaker (120 rpm for 20  
6 min) at 37°C, the supernatant was collected by centrifugation (3000g for 8 min at RT), resuspended in 2 mL  
7 DMEM/10% FBS, and seeded in the same medium either on poly-L-lysine-coated coverslips (15×15 mm; 2×10<sup>5</sup>  
8 cells/coverslip) for immunocytochemistry or in poly-L-lysine-coated Petri dishes (60 mm × 15 mm; 10<sup>6</sup>  
9 cells/dish) for Western blot analysis. The number of cells collected was determined in a Bürker chamber after  
10 trypan blue staining. DMEM/10% FBS was replaced the next day and then on the third and sixth day of  
11 subcloning (subDIV6).  
12  
13  
14  
15  
16  
17

18 Primary DIV6 co-cultures and microglia subDIV6 monocultures were challenged with lipopolysaccharide  
19 (LPS, dissolved in DMEM, 20 ng/mL in final concentration; Sigma, St. Louis, MO, USA) (Kata et al., 2016) and  
20 treated with nimodipine (dissolved in ethanol, 5 µM, 10 µM, 20 µM in final concentration; Sigma, St. Louis,  
21 MO, USA) on day 6. The following experimental conditions were established: (i) control (unchallenged,  
22 untreated), (ii) activated (challenged with LPS alone) for 24 h, (iii) treated with nimodipine alone (at 5, 10 and  
23 20 µM final concentrations) for 24 h, and (iv) challenged with LPS at the presence of nimodipine (5, 10 and  
24 20 µM final concentrations), LPS and nimodipine applied in combination for 24 h.  
25  
26  
27  
28  
29  
30

### 31 *Immunohistochemistry – cell cultures and brain slice preparations*

32 For immunohistochemistry, we used a protocol described previously (Kata et al., 2016). Briefly, primary  
33 co-cultures (DIV7) and microglia (subDIV7) monocultures on poly-L-lysine-coated coverslips were used for  
34 immunohistochemistry. Cells were fixed in 4% formaldehyde in 0.05 M phosphate buffered saline (PBS, pH 7.4  
35 at RT) for 5 min, then rinsed in 0.05 M PBS for 3 x 5 min. After permeabilization and blocking of nonspecific  
36 sites in 0.05 M PBS solution containing 5% normal goat serum (Sigma) and 0.3% Triton X-100 for 60 min at  
37 37°C, the cells on the coverslips were incubated overnight at 4°C with the appropriate primary antibodies  
38 (Table S1) in 1% heat-inactivated bovine serum albumin (BSA; Sigma) and 0.3% Triton X-100. The cultured cells  
39 were washed 3 x 5 min at RT in 0.05 M PBS, then incubated with the appropriate Alexa Fluor fluorochrome-  
40 conjugated secondary antibody (Table S1) in the above solution, but without Triton X-100, for 2 h at RT in the  
41 dark. The cells on the coverslips were washed in 0.05 M PBS for 3 x 5 min at RT, and the nuclei were stained  
42 in 0.05 M PBS solution containing 1 mg/ml polyvinylpyrrolidone and 0.5 µl/ml 2-(4-amidinophenyl)-1H-indole-  
43 6-carboxamide (DAPI; Thermo Fisher Scientific, Waltham, MA, USA). The coverslips were rinsed in distilled  
44 water for 5 minutes, air dried, and mounted on microscope slides in Vectashield mounting medium (Vector  
45 Laboratories, Burlingame, CA, USA).  
46  
47  
48  
49  
50  
51  
52  
53  
54  
55

56 Brain slices (350 µm) were rinsed with PBS, cryoprotected in 30% sucrose in PBS, embedded in paraffin,  
57 and sectioned (3 µm) on a rotation microtome (Leica RM 2235 Germany), as previously described (Frank et  
58  
59  
60

1  
2  
3 al., 2024). Sections were mounted on microscope slides, deparaffinized, and hydrated. Sections were then  
4 blocked with 10% normal goat serum (Sigma Aldrich, USA) for 1 hour at RT and incubated with rabbit anti-Iba1  
5 primary antibody (Table S1) overnight at 4°C. Sections were rinsed with PBS, incubated with goat anti-rabbit  
6 secondary antibody (Table S1) at RT for 2 hours in the dark, then rinsed with PBS and distilled water. Sections  
7 were finally coverslipped with Fluoromount G (Thermo Fisher, USA., 00-4959-52) containing DAPI. Microscopic  
8 images of the parietal cortex and the striatum were taken with a LEICA DFC250 camera (Leica Microsystems  
9 Wetzlar GmbH, Wetzlar, Germany) attached to a fluorescence microscope (40× magnification, Leica DM LB2,  
10 Leica Microsystems CMS GmbH, Wetzlar, Germany).

#### 11 12 13 14 15 16 17 18 *Western blot analysis – cell cultures*

19  
20 Cultured cells from primary co-cultures (DIV7) and microglial (subDIV7) monocultures were harvested  
21 with a rubber policeman, homogenized in 50 mM Tris-HCl (pH 7.5) containing 150 mM NaCl, 0.1% Nonidet  
22 P40, 0.1% cholic acid, 2 µg/ml leupeptin, 1 µg/ml pepstatin, 2 mM phenylmethylsulphonyl fluoride, and 2 mM  
23 EDTA, and centrifuged at 10,000g for 10 min at 4 °C. The pellet was discarded and the protein concentration  
24 of the supernatant was determined (Lowry et al., 1951). For quantitative analyses of microglial, neuronal,  
25 astrocyte, or oligodendrocyte immunoreactivity, 5-10 µg of protein was separated on a sodium dodecyl  
26 sulphate (SDS)-polyacrylamide gel (4-10% stacking gel/resolving gel), transferred to a Hybond-ECL  
27 nitrocellulose membrane (Amersham Biosciences, Little Chalfont, Buckinghamshire, England), blocked for 1  
28 hour in 5% non-fat dry milk in Tris-buffered saline (TBS) containing 0.1% Tween-20 and incubated overnight  
29 with the appropriate primary antibodies (Table S1) as well as the internal control (mouse anti-GAPDH  
30 monoclonal antibody). After rinsing 5 times in 0.1% TBS-Tween-20, the membranes were incubated with the  
31 appropriate peroxidase-conjugated secondary antibodies (Table S1) for 1 hour and washed 5 times. The  
32 enhanced chemiluminescence method (ECL Plus Western blotting detection reagents; Amersham Biosciences)  
33 was used to detect immunoreactive bands according to the manufacturer's protocol.

#### 34 35 36 37 38 39 40 41 42 43 44 45 *In vitro phagocytosis assay – cell cultures*

46  
47 The fluid-phase phagocytic capacity of microglial cells in primary co-cultures (DIV7) and microglial  
48 (subDIV7) monocultures was determined by uptake of fluorescent microspheres (2 µm diameter; Sigma, St.  
49 Louis, MO, USA). Briefly, 1 µL per millilitre of a 2.5% aqueous suspension of fluorescent microspheres was  
50 added to the cultures, which were then incubated at 37°C for 60 minutes. The cells were then rinsed five times  
51 with 2 mL of PBS to remove any residual fluorescent microspheres bound to the dish or cell surface, and fixed  
52 with 4% formaldehyde in 0.05 M PBS (pH 7.4 at RT) (Kata et al., 2016; Szabo et al., 2013).

#### 53 54 55 56 57 58 59 *Enzyme-linked immunosorbent assay (ELISA) – cell cultures*

1  
2  
3 The concentrations of interleukin-10 (IL-10) (ER0033, FineTest) and tumor necrosis factor- $\alpha$  (TNF- $\alpha$ )  
4 (ER1393, FineTest) in both primary co-cultures (DIV7) and microglial (subDIV7) monoculture supernatants  
5 derived from the Western blot experiments were analysed using an ELISA kit according to the manufacturer's  
6 instructions. An automated microplate reader (Multiskan FC with the software SkanIt RE 5.0, Thermo  
7 Scientific) was used to measure optical density (OD) at 450 nm. The concentration of each sample was  
8 determined based on the optical density and the concentration of the standard. According to the  
9 manufacturer, the overall intra-assay and coefficient of variation were <8% for both IL-10 and TNF- $\alpha$ , and the  
10 inter-assay was <10% for both IL-10 and TNF- $\alpha$ .  
11  
12  
13  
14  
15  
16  
17

#### 18 *NEB mRNA-Library and high-throughput sequencing – cell cultures*

19  
20 Microglial monocultures were selected for gene expression analysis because the effect of nimodipine on  
21 microglial activation was essentially the same in both co-cultures and monocultures, and cell separation was  
22 not required for monocultures. Because 10  $\mu$ M nimodipine was the lowest effective concentration of the drug  
23 on microglial activation, we focused the gene expression analysis on this treatment.  
24  
25

26  
27 Cortical brain tissue was collected from 3-5 litters (30 pups), males and females mixed. Tissue was pooled  
28 and processed for monocultures. The harvested tissue allowed the preparation of 3 biological replicates at a  
29 time. For bulk RNA sequencing (RNA-Seq), the three biological replicates were assigned to the three  
30 experimental groups: control, LPS alone and LPS+nimodipine, were run in parallel and each yielded a sample  
31 of ~1 million cells. This was repeated three times to provide three biological replicates for each of the three  
32 experimental groups. Total RNA was isolated from the collected cells with RNeasy Mini Kit (74104 Qiagen)  
33 using 1 million cells/sample. Total RNA samples were quantified with Qubit 3.0 Fluorometer (ThermoFisher)  
34 and quality checked with Tape Station 4200 instrument using Agilent RNA ScreenTape (Agilent Technologies  
35 USA, Cat. No. 5067-5576).  
36  
37  
38  
39  
40  
41

42 NGS library preparation was carried out using the NEBNext Ultra™ II Directional RNA Library Prep Kit for  
43 Illumina (NEB #E7760) with NEBNext Poly(A) mRNA Magnetic Isolation Module (NEB #E7490). After mRNA  
44 enrichment, cDNA was generated where a second strand synthesis was done with the dUTP method to retain  
45 strand specificity. Finally, double-stranded cDNA was end-prepped and Illumina-specific adaptors were ligated  
46 to the cDNA fragments, followed by a final enrichment PCR.  
47  
48  
49

50 Sequencing ready libraries were quality control checked by Tape Station 4200 instrument using D5000  
51 ScreenTape (Agilent Technologies USA, Cat. No. 5067-5588). Next generation sequencing was carried out on  
52 NovaSeq X Plus sequencing system with NextSeq NovaSeq X Series 10B Reagent Kit (300 Cycle) chemistry  
53 (Illumina, Inc. USA, 20085594).  
54  
55  
56  
57

#### 58 *Image analysis – cell cultures and brain slice preparations*

1  
2  
3 Digital images were captured using a LEICA DFC250 camera (Leica Microsystems Wetzlar GmbH, Wetzlar,  
4 Germany) attached to a fluorescence microscope (Leica DM LB2, Leica Microsystems CMS GmbH, Wetzlar,  
5 Germany) and LAS X Application Suite (Leica Microsystems CMS GmbH, Wetzlar, Germany). To determine the  
6 purity of microglial cells, DAPI-labelled nuclei of Iba1-immunopositive cells were counted. In cell cultures, at  
7 least two coverslips from each experiment were analysed, with approximately 20 randomly selected cells per  
8 coverslip in three separate experiments. In brain slices, five cells from both cortex and striatum were analysed  
9 from six coverslips per group. Microglial cell silhouettes were obtained by converting the raw digital files of  
10 Iba1-immunoreactive cells captured by fluorescence microscopy into binary files using Adobe Photoshop CS3  
11 software (Adobe Systems, Inc., San Jose, CA, USA). After binary conversion, cell perimeter and area of  
12 individual cells were measured in ImageJ (National Institutes of Health, Bethesda, MD, USA) and the TI  
13 reflecting the degree of process extension was calculated as follows:  $\text{perimeter}^2/\text{area} * 4\pi$  as previously  
14 described (Szabo and Gulya, 2013). A total of 420 cell silhouettes were analysed in this study.

15  
16 To measure phagocytic activity, cells were labelled with phagocytosed microbeads. The microbeads in the  
17 cytoplasm were counted. Twenty non-overlapping random fields were captured using a fluorescence  
18 microscope with a 40x objective (Leica DMLB epifluorescence microscope), and the microbead load of a total  
19 of 100 cells in each culture was evaluated using the ImageJ cell counter plugin (National Institutes of Health,  
20 Bethesda, MD, USA). The mean microbead count of 100 cells was taken as a single value representing each  
21 culture.

22  
23 Gray-scale digital images of the immunoblots were obtained by scanning the autoradiographic films with  
24 a desktop scanner (Epson 430 Perfection V750 PRO; Seiko Epson Corp., Suwa, Japan). Images were scanned  
25 and processed with identical settings to allow comparison of blots from different samples. The bands were  
26 outlined and analysed by densitometry using ImageJ (National Institutes of Health, Bethesda, MD, USA).  
27 Immunoreactive densities of equally loaded lanes were quantified as we previously reported (Kata et al.,  
28 2016). Samples were normalized to the densities of internal controls (GAPDH) and presented as % of controls.

#### 29 30 31 32 33 34 35 36 37 38 39 40 41 42 43 44 45 *Statistical analysis*

46  
47 The data and statistical analyses complied with the recommendations of the British Journal of  
48 Pharmacology for experimental design and analysis in pharmacology (Curtis et al., 2022), wherein the smaller  
49 n number used here is deemed exploratory. Statistical comparisons for microglial morphology, Western blot,  
50 phagocytic activity, and ELISA assay were performed using GraphPad Prism 8.0 (Windows, GraphPad Software,  
51 San Diego, California USA, [www.graphpad.com](http://www.graphpad.com)). Normality of data distribution was determined by the  
52 Shapiro-Wilk test. In case of normal distribution of data, one-way analysis of variance (ANOVA) followed by  
53 Tukey's multiple comparison test was used for statistical analysis, and data were presented as mean $\pm$ stdev in  
54  
55  
56  
57  
58  
59  
60

1  
2  
3 bar graphs. In case of non-normal distribution of data, Kruskal-Wallis test followed by Dunn's multiple  
4 comparison was used and data were presented in box plots. The significance level was set at  $p < 0.05$ .

5  
6 For the processing of RNA-Seq data, the quality of the pair-ended reads was performed using FastQC  
7 (0.12.1) (Andrews, 2010), while adapters and low-quality bases were trimmed using FASTP (0.23.4) (Chen et  
8 al., 2018). The filtered reads were aligned to the *Rattus norvegicus* genome (NCBI: GRCr8) using the splice-  
9 aware aligner, STAR (2.5.2b) (Dobin et al., 2013), and quantified with FeatureCounts (v.2.0.6) (Liao et al., 2014).  
10 For the downstream analysis, only genes with a CPM (counts per million) greater than 2 in at least three  
11 samples were retained. The filtered samples were then normalized using the TMM (Trimmed Mean of M-  
12 values) method implemented in edgeR's calcNormFactors (v.4.0.16) function (Robinson et al., 2010).  
13 Differential gene expression analysis was performed using limma-voom (Law et al., 2014).  
14  
15  
16  
17  
18  
19

20 PCA and hierarchical clustering were used to examine the similarities between samples and identify  
21 potential outliers. Differently expressed genes (DEGs) were identified for the following comparisons: (i) LPS  
22 vs. Control, (ii) LPS+nimodipine vs. Control, and (iii) LPS+nimodipine vs. LPS. In each comparison, DEGs were  
23 defined as those with a log<sub>2</sub> fold change greater than 1 and an adjusted p-value  $< 0.05$ .  
24  
25  
26

27 To assess the effects of different treatments on gene expression, we selected genes from various  
28 pathways and analysed their expression changes. Log Fold Change and p-values were used to evaluate the  
29 differential expression of these genes across comparisons. We identified significantly upregulated and  
30 downregulated genes based on three significant levels for these pathways. Additionally, heatmaps were  
31 generated for each pathway to provide a detailed view of expression patterns. The complete results of this  
32 analysis, including all significant genes, are available in the supplementary materials.  
33  
34  
35  
36  
37

## 38 Results

### 39 *Nimodipine alters the morphological phenotype of activated microglia*

40  
41  
42 First, we extended our findings made previously in metabolically challenged live brain slice preparations  
43 (Frank et al., 2024). The morphological phenotype of microglia corresponds to the state of activation, with a  
44 ramified morphology associated with the quiescent state and an amoeboid shape indicating activation.  
45 Microglia acquired an apparent amoeboid, activated morphological phenotype upon mOGD (TI values in the  
46 range of 3-5) (Fig. 1). Nimodipine (10  $\mu$ M) partially restored the ramified morphology in both the cerebral  
47 cortex and striatum in the mOGD-challenged brain slices (TI values in the range of 8-9) (Fig. 1).  
48  
49  
50  
51  
52  
53  
54  
55  
56  
57  
58  
59  
60

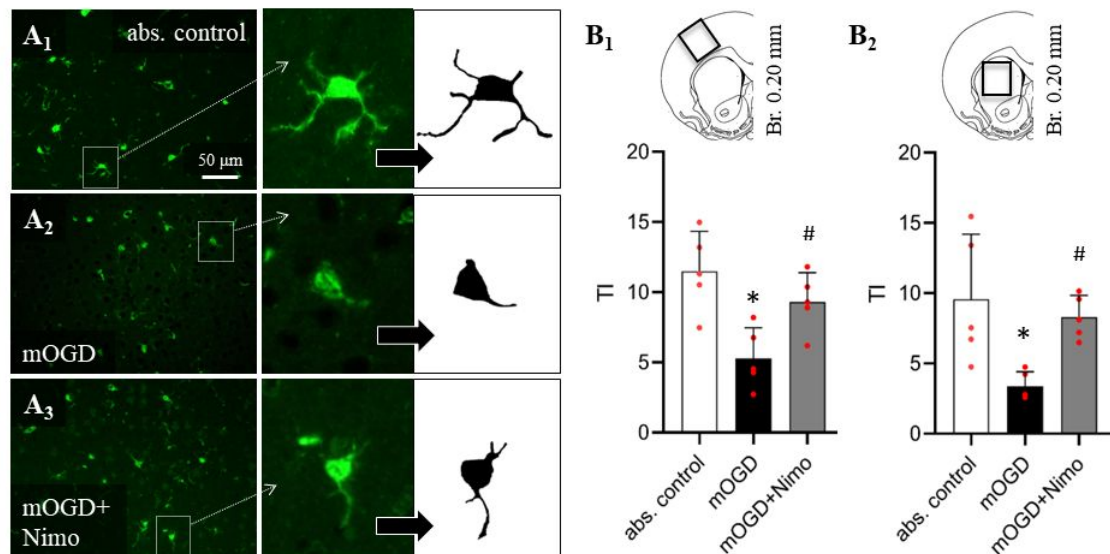


**Figure 1.** Quantitative analysis to evaluate the effect of nimodipine on microglial morphology in live brain slice preparations. **A**, Fluorescence immunohistochemistry images show Iba1-labeled microglia in absolute control brain slices (A<sub>1</sub>), in slices exposed to mild oxygen glucose deprivation (mOGD) (A<sub>2</sub>), and to mOGD in combination with nimodipine (mOGD+Nimo) (A<sub>3</sub>) in the cerebral cortex. Binary silhouettes of individual Iba1-positive microglia show the arborization of the cells. **B**, Transformation index (TI) calculated to quantify the degree of arborization (decreasing TI corresponds to an amoeboid shape and thus increasing activity) in the cortex (B<sub>1</sub>) and striatum (B<sub>2</sub>). Data were obtained as follows: The morphological phenotype of 15 microglia per brain slice were evaluated and the average was taken as a single data point. Five brain slices were analysed in each of the 3 experimental groups. Data are presented as mean±stdev (n=5/group). Normality of data distribution was determined by Shapiro-Wilk test (B<sub>1</sub>: p= 0.867; B<sub>2</sub>: p= 0.857). Data were analysed by one-way analysis of variance (ANOVA) (B<sub>1</sub>, f= 8.723, p=0.0046\*; B<sub>2</sub>, f= 6.501, p=0.0122\*) followed by Holm-Sidak's multiple comparisons test (p<0.05\* vs. abs. control; p<0.05# vs. mOGD).

To explore nimodipine's direct effect on microglia, microglial cell cultures were used. In the untreated co-cultures, microglia typically exhibited a quiescent morphology, with small pseudopodia (Fig 2A-B). In microglial monocultures, the cells were slightly more ramified with TI ~4 (Fig. 2C-D). Activation with LPS significantly decreased TI in both co-cultures and monocultures, corresponding to an amoeboid morphological phenotype (Fig. 2). When applied to non-activated cultures, nimodipine (5, 10, 20 μM) induced the formation of numerous microspikes (filopodia) in both co-cultures and monocultures (Fig. 2A, C), but did not result in significantly increased TI values (Fig. 2B, D). The addition of nimodipine to LPS-activated cultures increased microglial TI close to control levels, especially at 10-20 μM concentrations, and resulted in a more quiescent phenotype in both co-cultures and monocultures (Fig. 2). This indicates that nimodipine at concentrations of 10 and 20 μM effectively counteracted the morphological changes characteristic of LPS-induced microglial activation.

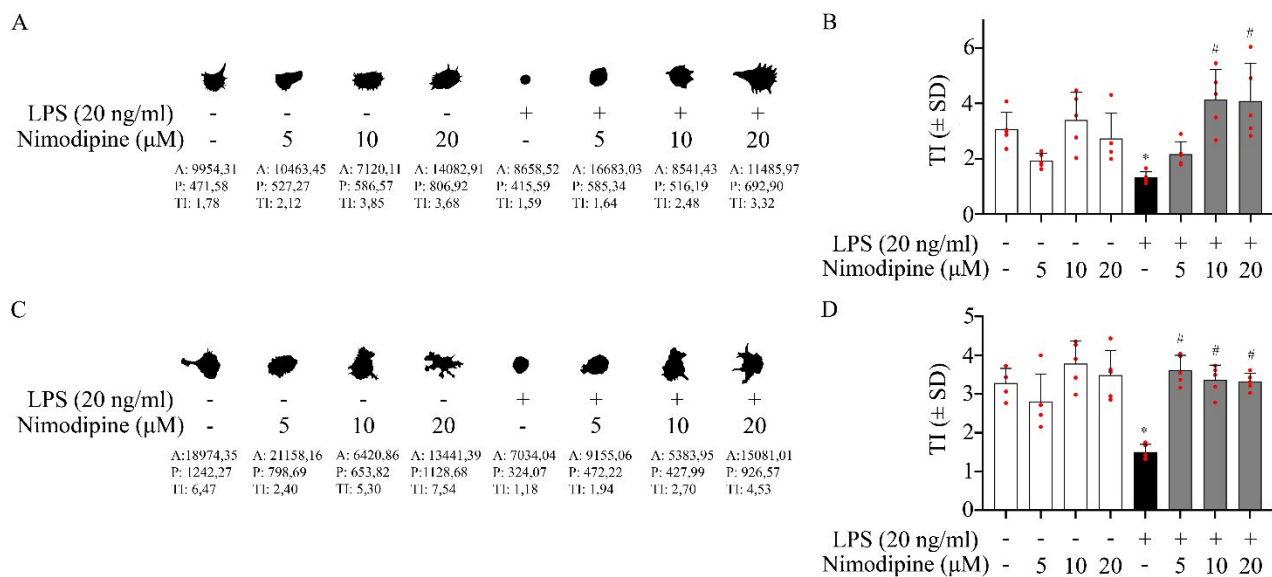


**Figure 2.** Quantitative analysis to evaluate the effect of nimodipine on microglial morphology in co-cultures (A-B) and microglia monocultures (C-D). **A**, Iba1-positive cell masks representative of microglia in co-cultures (DIV7). **B**, Microglial transformation index (TI) calculated for each experimental condition in co-cultures. **C**, Iba1-positive cell masks representative of microglia in mono-cultures (subDIV7). **D**, Transformation index (TI) calculated for each experimental condition in microglia mono-cultures. In A and C, the values are given below the masks: A, area; P, perimeter; TI, transformation index. In B and D, data were obtained as follows: The morphological phenotype of 15 randomly selected microglia per culture were evaluated and the average was taken as a single data point. Five cell cultures were analysed in each of the 8 experimental groups. Data are presented as mean $\pm$ stdev; red spheres represent individual values in each condition (n=15/experimental condition). Normality of the data distribution was determined by the Shapiro-Wilk test (B, p=0.340; D, p=0.532). Data were analysed by one-way analysis of variance (ANOVA) (B, f=7.419, p<0.05\*; D, f=11.880, p<0.05\*) followed by Tukey's multiple comparison (p<0.05\* vs. absolute control; p<0.05# vs. LPS alone).

#### Nimodipine reduces microglial Iba1 levels after activation

Microglial Iba-1 expression was taken as an indicator of activation. Western blot analysis showed that Iba-1 levels were increased in LPS-treated co-cultures (169.0 $\pm$ 33.7 % of control) and monocultures (213.4 $\pm$ 29.7 % of control) compared to the non-activated control condition (Fig. 3). Nimodipine did not alter Iba1 levels in non-activated cultures. In contrast, in LPS-activated co-cultures, the addition of nimodipine resulted in a concentration-dependent reduction of Iba1 expression (103.7 $\pm$ 8.3 and 64.9 $\pm$ 15.9 vs. 169.0 $\pm$ 33.7 % of control, LPS + 10 and 20  $\mu$ M nimodipine vs. LPS) (Fig. 3B). In microglia monocultures, nimodipine reduced Iba1 levels to control at all three concentrations used (95.3 $\pm$ 18.1, 108.3 $\pm$ 20.1 and 77.2 $\pm$ 8.5 vs. 213.4 $\pm$ 29.7 % of control, LPS + 5, 10 and 20  $\mu$ M nimodipine vs. LPS) (Fig. 3D).

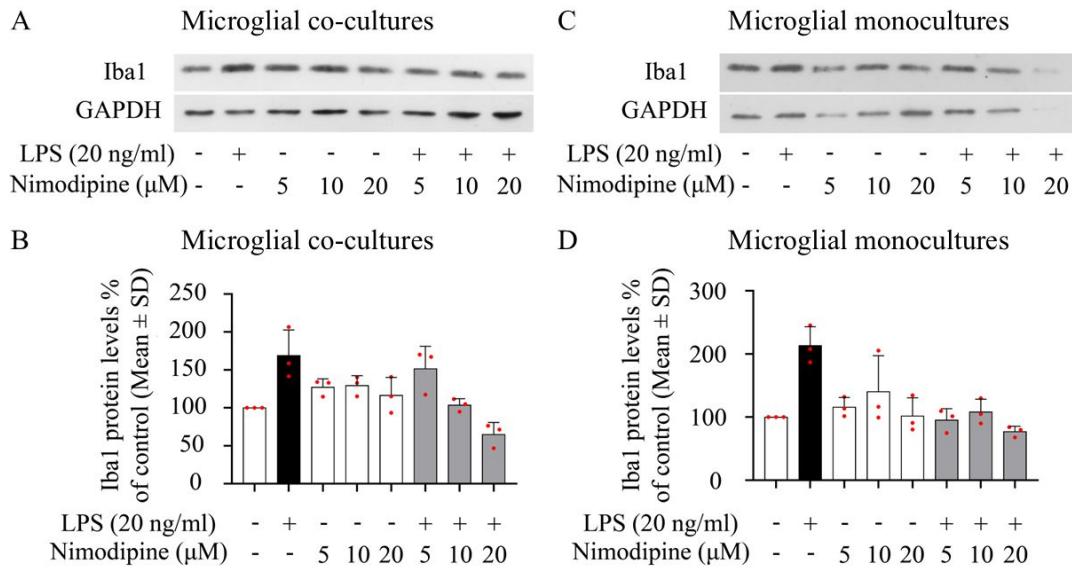
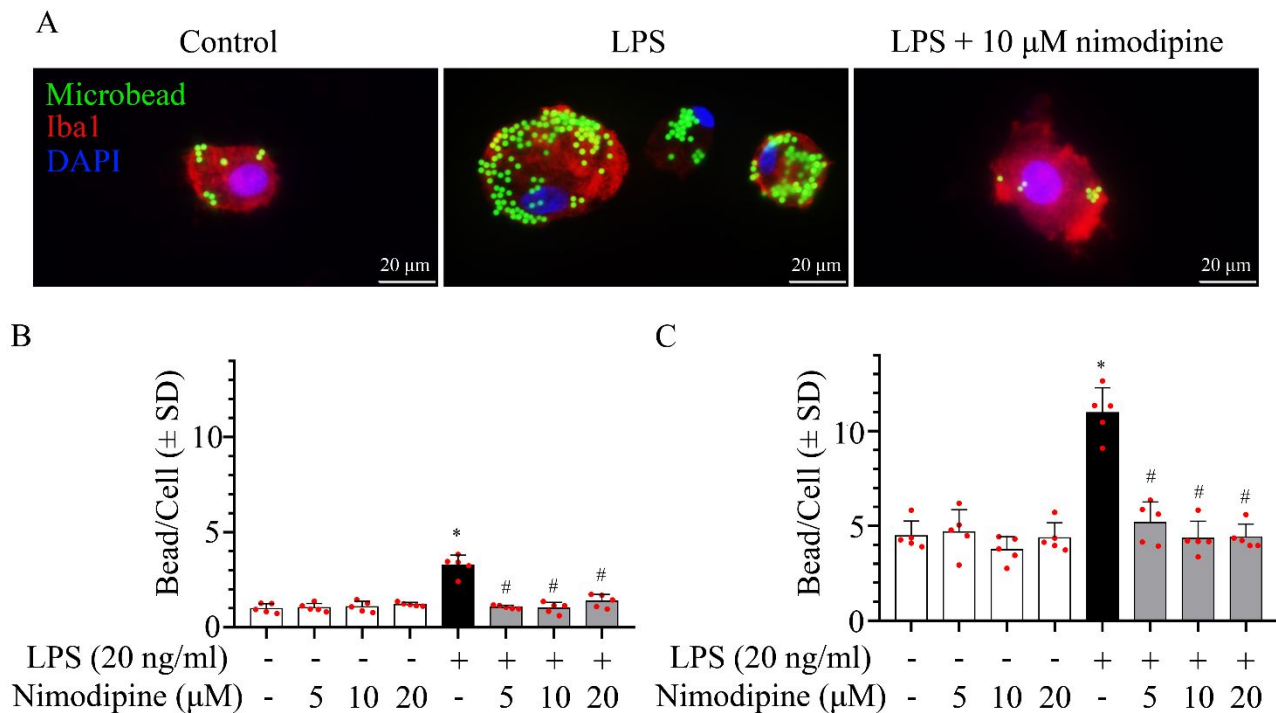


**Figure 3.** Exploratory quantitative analysis to detect the effect of nimodipine on microglial Iba1 protein levels in co-cultures (A-B) and microglial monocultures (C-D). **A**, Representative Western blot images for Iba1 and GAPDH, used as an internal control, obtained from co-cultures. **B**, Iba1 protein levels quantified in co-cultures. **C**, Representative Western blot images for Iba1 and GAPDH from microglial monocultures. **D**, Iba1 protein levels quantified in microglia monocultures. In A and C, images were scanned and processed with identical settings to allow comparisons between Western blots from different samples. In B and D, data are integrated optical density values relative to control, and the descriptive statistics present data as mean±stdev. Red spheres indicate individual values (n=3) in each group.

#### *Nimodipine reduces phagocytic activity of activated microglia*

Microglia in control cultures exhibited low levels of phagocytosis, engulfing only  $0.9 \pm 0.3$  microbeads per cell in co-cultures and  $4.7 \pm 1.0$  in monocultures. Phagocytosis was typically seen in amoeboid microglia in all experimental conditions, whereas ramified microglia rarely contained microbeads, as seen previously (Szabo and Gulya, 2013). Nimodipine applied to non-activated cultures had no significant effect on phagocytosis, with the number of phagocytosed microbeads remaining low (co-cultures:  $1.19 \pm 0.2$ ; monocultures:  $4.21 \pm 1.2$  microbeads per cell). As expected, LPS significantly increased microglial phagocytic activity. On average, LPS-activated microglia accumulated  $3.5 \pm 0.3$  microbeads per cell in co-cultures and  $11.5 \pm 1.2$  microbeads per cell in monocultures. The addition of nimodipine significantly inhibited phagocytosis, which returned to near control levels in both co-cultures ( $1.29 \pm 0.15$  microbeads per cell) and in monocultures ( $4.63 \pm 1.14$  microbeads per cell) (Fig. 4).



28  
29  
30  
31  
32  
33  
34  
35  
36  
37  
38  
39

**Figure 4.** Evaluation of the effect of nimodipine on microglial phagocytic activity as visualized by fluorescent microbeads co-localized with Iba1 protein. **A**, Representative fluorescence microscopic images of Iba1-labeled microglia in monocultures. Fluorescent microbeads in their cytoplasm indicate increased phagocytic activity after LPS activation, which was counteracted by nimodipine. **B**, Phagocytotic activity of microglia quantified in co-cultures. **C**, Phagocytotic activity quantified in microglial monocultures. Note, that phagocytosis was typically seen in activated, amoeboid cells in all experimental groups. In B and C, data were obtained as follows: The morphological phenotype of 100 microglia per culture dish were evaluated and the average was taken as a single data point. Five cell cultures were analysed in each of the 8 experimental groups. Data are presented as mean $\pm$ stdev; red spheres represent individual cultures in each group. Normality of data distribution was determined by Shapiro-Wilk test (B,  $p=0.289$ ; C,  $p=0.264$ ). Data were analysed by one-way analysis of variance (ANOVA) (B,  $f=34.76$ ,  $p<0.05^*$ ; C,  $f=30.42$ ,  $p<0.05^*$ ) followed by Tukey's multiple comparison ( $p<0.05^*$  vs. absolute control;  $p<0.05^{\#}$  vs. LPS alone).

#### 40 Nimodipine reduces the secretion of TNF- $\alpha$ by activated microglia

41  
42  
43  
44  
45  
46  
47  
48  
49  
50  
51

Activated microglia express both pro- and anti-inflammatory cytokines. Here, we evaluated the levels of the pro-inflammatory cytokine TNF- $\alpha$  and the anti-inflammatory cytokine IL-10 in the culture media. The basal level of IL-10 was  $146.98\pm 24.19$  pg/ml in co-culture media and  $144.5\pm 7.89$  pg/ml in monoculture media. LPS at the low concentration used (20 ng/ml) did not significantly alter IL-10 protein expression ( $180.26\pm 0.87$  and  $123.25\pm 65.59$  pg/ml, co-cultures and monocultures, respectively). Nimodipine had no effect on IL-10 levels in either non-activated or activated cultures.

52  
53  
54  
55  
56  
57  
58  
59  
60

The level of TNF- $\alpha$  was  $5.37\pm 1.64$  pg/ml in non-activated co-cultures and  $6.74\pm 3.43$  pg/ml in monocultures (Fig. S1). Low dose LPS activation did not significantly change the TNF- $\alpha$  concentration measured at 24 h (peak values expected at 6 h, Kata et al., 2016), despite a visible tendency to increase both in co-cultures (from  $5.37\pm 1.64$  to  $15.52\pm 4.95$  pg/ml) and in monocultures (from  $6.74\pm 3.43$  to  $33.35\pm 17.26$  pg/ml). Again, nimodipine had no effect on non-activated cultures. However, nimodipine (20  $\mu$ M) reduced TNF- $\alpha$

concentration in LPS-activated co-cultures to the control levels ( $1.61 \pm 0.41$  pg/ml). In LPS-activated monocultures, nimodipine produced a stepwise reduction in TNF- $\alpha$  levels along its increasing concentration (27.76 $\pm$ 19.54, 23.25 $\pm$ 12.27 and 13.61 $\pm$ 10.26 pg/ml, 5, 10 and 20  $\mu$ M, respectively), although without statistical significance.

### LPS markedly alters gene expression indicating pro-inflammatory microglial phenotype

High-throughput RNA sequencing was conducted on microglial monocultures. Principal component analysis (PCA) of the transcriptome data showed that replicates of the control group clustered closely together, and the LPS- and LPS+nimodipine-treated samples were clearly separated from the control. The LPS and LPS+nimodipine samples were heterogeneous and did not form distinct clusters, revealing a predictably weaker effect of nimodipine on gene expression than that of LPS (Fig. S2). The PCA results were reflected in the unsupervised hierarchical clustering of the samples (Fig. S2). In total, 13,866 genes were identified by bulk RNA sequencing in primary microglial monocultures, of which 9,720 were differentially expressed (DEGs) by LPS challenge alone or in combination with nimodipine treatment (Fig. 5).

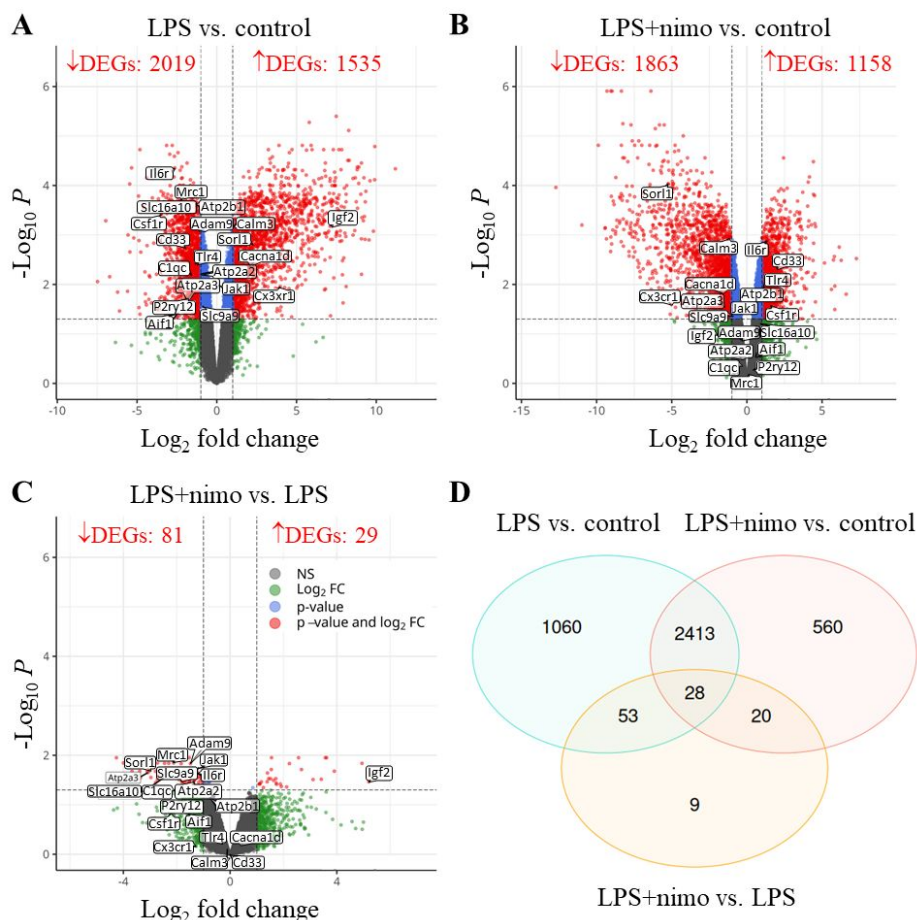


**Figure 5. Activation with lipopolysaccharide (LPS) and treatment with nimodipine (nimo) cause alterations in rat primary microglia transcriptome.** Volcano plots depict  $\text{Log}_2$  fold changes and  $-\text{Log}_{10}$  of the adjusted p-value per gene comparing LPS vs. control (A), LPS+nimodipine treatment vs. control (B) and LPS+nimodipine treatment vs. LPS alone (C). Venn diagram shows the overlap of differentially expressed genes (DEGs) in the three experimental conditions (D). Cutoff values are  $\text{Log}_2\text{FC}=1$  and  $p=0.05$ .

1  
2  
3 We identified the *Cacna1c* and *Cacna1d* gene transcripts, encoding the Cav1.2 and Cav1.3 pore-forming  
4  $\alpha$  subunits of LVGCCs, the target of nimodipine. The short-read RNA sequencing performed here did not  
5 provide definitive evidence of truncation. However, several splice variants of *Cacna1c* and *Cacna1d* were  
6 identified (Table S2).  
7  
8

9  
10 Next, we analyzed gene expression patterns linked to distinct functions of activated microglia. LPS is  
11 specifically recognized by toll-like receptor 4 (TLR4) receptors located on the microglial plasma membrane  
12 (Lenhardt et al., 2003). Indeed, the expression of the TLR4 gene (*Tlr4*) was significantly upregulated in the LPS-  
13 challenged microglia. Downstream of TLR4, the expression of several genes encoding adaptor proteins of TLR4  
14 signalling cascades (Zhou et al., 2020) were all upregulated (e.g. *Myd88*, *Ticam1*, *Ticam2*) (Fig. S3).  
15  
16

17  
18 Further, LPS considerably enhanced cytokine signalling in the primary microglial cultures. Specific genes  
19 encoding interleukins and chemokines were upregulated (e.g. *Il7*, *Il11*, *Il16*, *Il18*, *Ccl20*, *Cxcl6*, *Cxcl16*), while  
20 others were downregulated (e.g. *Il17d*, *Il34*, *Ccl19*, *Cxcl12*, *Cxcl14*) (Fig. S4). The gene expression of a group of  
21 cytokine receptors was also significantly upregulated (e.g. *Il1r1*, *Il6r*, *Il7r*, *Il23r*, *Tnfrsf1b*, *Tnfrsf8*, *Tnfrsf25*,  
22 *Tnfrsf26*) (Fig. S4). Microglia have traditionally been classified according to their state of activation as  
23 quiescent M0 or activated on a phenotypic spectrum between M1 and M2, with M1 being pro-inflammatory  
24 and M2 neuroprotective. Some of the markers previously recognized to represent M1 polarization (Jurga et  
25 al., 2020) were expressed at significantly higher levels (e.g. *Ccl20*, *Cd86*, *Il18*), whereas gene expression typical  
26 for M2 polarization (e.g. *Il10*, *Ccl2*, *Ccl22*, *Cxcl13*, *Arg1*) (Jurga et al., 2020) was not altered in the LPS-activated  
27 cultures, suggesting a predominantly pro-inflammatory microglial phenotype (Fig. S4).  
28  
29

30  
31 In addition to the widely appreciated cytokine response of microglia to pathogen- or damage-associated  
32 molecular patterns, microglia release complement components and express complement receptors, which  
33 contribute to pathological mechanisms in neurodegenerative disorders (Chen et al., 2022). Of the first  
34 elements of the classical complement cascade, the LPS challenge upregulated genes of the complement  
35 component C1q (*C1qa* and *C1qc*) and downregulated complement components *C1r* and *C1s*. Downstream the  
36 classical pathway, complement components *C4a* and *C4b* were also expressed at significantly lower levels. On  
37 the other hand, the expression of complement receptor genes *C3ar1* and *C5ar1* were markedly upregulated  
38 by LPS (Fig. S5).  
39  
40

41  
42 Consistent with the increased phagocytic activity in response to LPS shown here (Fig. 4), the expression  
43 levels of phagocytic receptor genes (Podleśny-Drabiniok et al., 2020; Thomas et al., 2022) were significantly  
44 increased (e.g. *Mertk*, *Trem1*, *Cd14*, *Cd33*, *Cd68*, *Ms4a4a*), except for *Sorl1*, which was downregulated  
45 (Fig. S6). Autophagy, a catabolic mechanism to degrade dysfunctional proteins and organelles may suppress  
46 inflammation (Jin et al., 2018). The expression of genes associated with macroautophagy (e.g. *Mtor*, *Ulk1*,  
47 *Atg6l*, *Map1lc3b* or *Sqstm1*), however, were not affected by LPS. Yet, the genes of some proteins that regulate  
48 autophagy (e.g. *Wdfy3* and *Dnajc16*) were expressed at a higher level due to LPS.  
49  
50  
51  
52  
53  
54  
55  
56  
57  
58  
59  
60

1  
2  
3 Finally, as recently reported (Sabogal-Guáqueta et al., 2023), LPS induced a metabolic shift in cultured  
4 microglia. In general, genes encoding glycolytic enzymes were upregulated, whereas genes of some enzymes  
5 of the TCA cycle were downregulated (Fig. S7). In particular, hexokinase genes (Hk2 and Hk3) were expressed  
6 at higher levels, in line with previous reports (Sabogal-Guáqueta et al., 2023), indicating the potential for  
7 increased glucose phosphorylation.  
8  
9

#### 10 11 12 13 *LPS modifies intracellular calcium homeostasis with distinct action of nimodipine*

14  
15 Because microglia respond to stimulation with intracellular  $\text{Ca}^{2+}$  accumulation, and nimodipine is a  
16 calcium channel blocker, we analysed how proteins implicated in intracellular  $\text{Ca}^{2+}$  homeostasis are altered by  
17 LPS and nimodipine.  
18  
19

20 Calcium influx across the plasma membrane in microglia is mediated by VGCCs, ligand-gated cation  
21 channels, transient receptor potential (TRP) cation channels, and  $\text{Ca}^{2+}$  release-activated  $\text{Ca}^{2+}$  channels (CRACs)  
22 (Fig. S8). The gene expression of many of these pathways of  $\text{Ca}^{2+}$  movement was altered by LPS. In particular,  
23 some of the genes of the pore-forming  $\alpha$  subunit of VGCCs were remarkably downregulated (Cacna1d,  
24 Cacna1e, Cacna1g, Cacna1h). Among the ligand-gated cation channels, the expression of the genes encoding  
25 the 3A subunit of the NMDA receptor (Grin3a) and subunits 1 and 2 of the AMPA receptor (Gria1 and Gria2)  
26 was decreased, while the expression of P2RX4 purinergic receptor (P2rx4) gene was increased. Nimodipine  
27 counteracted the LPS effect on the expression of the Gria1 gene. Regarding TRP channels, the expression of  
28 the gene of TRPM2 (Trpm2) was upregulated. With the addition of nimodipine, the LPS-induced upregulation  
29 of P2rx4 and Trpm2 was no longer evident (LPS+nimodipine vs. control). Finally, the gene Orai1, which encodes  
30 a CRAC, was not affected (Table 1).  
31  
32  
33  
34  
35  
36  
37

38 The endoplasmic reticulum (ER) is the major  $\text{Ca}^{2+}$  store in cells and is equipped with ligand-gated  
39 ryanodine receptors (RyRs) and inositol triphosphate receptors (IP3Rs) to mediate  $\text{Ca}^{2+}$  release upon activation  
40 (Fig. S8). In addition,  $\text{Ca}^{2+}$  pumps (SERCA) ensure  $\text{Ca}^{2+}$  uptake into the ER against the  $\text{Ca}^{2+}$  concentration  
41 gradient at the expense of ATP. The expression of all these genes was remarkably modulated by LPS treatment.  
42 Comparison of LPS-challenged microglia with the control showed that RyR genes (Ryr2-3) along with the IP3R  
43 genes (Itpr1-3) were downregulated. In contrast, the expression of the IP3R gene Itpr2 was upregulated by  
44 LPS. Genes encoding SERCA (Atp2a2 and Atp2a3) were remarkably upregulated by exposure to LPS.  
45 Interestingly, the effect of nimodipine treatment was apparent only on the genes upregulated by LPS.  
46 Comparing the LPS+nimodipine group with the LPS alone group, Itpr2, Atp2a2, and Atp2a3 were  
47 downregulated by nimodipine treatment (Table 1).  
48  
49  
50  
51  
52  
53  
54

55 Among the  $\text{Ca}^{2+}$  binding proteins, the gene of Iba1 (Aif1) was upregulated by LPS (Table 1), consistent with  
56 protein levels measured with Western blot analysis here (Fig. 3). Although nimodipine showed a tendency to  
57 counteract the LPS effect on Aif1 expression, the effect was not significant at mRNA level (Table 1) in contrast  
58  
59  
60

with a significant reduction at protein level (Fig. 3). The expression of the Calm3 gene coding for the calcium binding protein calmodulin 3 was markedly decreased by LPS, but nimodipine did not change the gene expression of calmodulins (Table 1).

**Table 1.** Changes in gene expression of calcium channels and calcium binding proteins in primary microglia monocultures.

		Gene	LPS vs. Control	LPS+nimo vs. Control	LPS+nimo vs. LPS
Voltage-gated channels	Cav2.1 (P/Q type)	<b>Cacna1a</b>	-0.7219*	-0.3948	0.3272
	Cav2.2 (N type)	<b>Cacna1b</b>	0.6013	0.7139	0.1126
	Cav1.2 (L type)	<b>Cacna1c</b>	-0.2578	0.3518	0.6097
	Cav1.3 (L type)	<b>Cacna1d</b>	-2.0082*	-1.6291*	0.3792
	Cav2.3 (R type)	<b>Cacna1e</b>	-6.3553*	-4.1933*	2.1620
	Cav3.1 (T type)	<b>Cacna1g</b>	-1.3216*	-1.4446*	-0.1231
	Cav3.2(T type)	<b>Cacna1h</b>	-4.3333*	-3.1830*	1.1503
Ligand gated ion channels	NMDA glutamate receptor subunits	<b>Grina</b>	-0.3575	0.2532	0.6107
		<b>Grin3a</b>	-5.7735*	-3.8086*	1.9649
		<b>Grin3b</b>	0.5822*	0.3713	-0.2109
		<b>Grin2d</b>	-0.4088	-0.4464	-0.0376
	AMPA glutamate receptor subunits	<b>Gria1</b>	-8.7561*	-5.1868*	3.5692*
		<b>Gria2</b>	-3.9386*	-7.4451*	-3.5065
		<b>Gria3</b>	0.4753	0.0275	-0.4479
Ionotropic purinergic receptors	<b>P2rx4</b>	1.1635*	0.4266	-0.7369	
	<b>P2rx5</b>	1.6848	1.9936	0.3088	
	<b>P2rx7</b>	-0.5053	0.5582	1.0635	
TRP channels	TRPM2	<b>Trpm2</b>	1.8575*	0.9351	-0.9225
	TRPM7	<b>Trpm7</b>	-0.0819	-0.1983	-0.1164
	TRPV1	<b>Trpv1</b>	0.9004	0.8205	-0.0799
Calcium release-activated calcium channel	<b>Orai1</b>	0.2527	1.0148	0.7621	
Endoplasmic reticulum	Ryr	<b>Ryr2</b>	-3.9591	-4.6406*	-0.6815
		<b>Ryr3</b>	-2.4677*	-1.4115*	1.0562
	Ip3R	<b>Itpr1</b>	-1.1016*	-1.3957*	-0.2941
		<b>Itpr2</b>	0.9807*	-0.2841	-1.2649*
	SERCA	<b>Itpr3</b>	-0.9831*	-1.2148*	-0.2317
		<b>Atp2a2</b>	1.0718*	-0.2831	-1.3549*
<b>Atp2a3</b>	1.5887*	-1.4889*	-3.0776*		
Mito-chondrium	Mitochondrial	<b>Mcu</b>	-0.6424*	-0.4994*	0.1429
	Calcium Uniporter subunits	<b>Mcub</b>	-0.0008	0.4497	0.4505
		<b>Mcur1</b>	0.0440	-0.4735	-0.5175
	NCX, member b1	<b>Slc8b1</b>	1.5158*	1.3136*	-0.2022
Calcium binding proteins	Iba1	<b>Aif1</b>	1.4998*	0.5662	-0.9336
		<b>Calm1</b>	-0.2130	0.4626	0.6757
		<b>Calm2</b>	-0.4094	-0.3885	0.0209
	Calmodulins	<b>Calm3</b>	-1.0347*	-1.1380*	-0.1033
		<b>Ppp3ca</b>	0.6170	0.6156	-0.0014
		<b>Ppp3cb</b>	-0.3496	-0.1691	0.1804
	Calcineurin subunits	<b>Ppp3cc</b>	-0.6994*	-0.3446	0.3549
		<b>Ppp3r1</b>	-0.1563	-0.0850	0.0713
		<b>Rcan1</b>	-0.0053	-0.4070	-0.4018

Upregulated      Downregulated      No change

Change in mRNA expression is expressed as Log<sub>2</sub>FC (adjusted p<0.05\*); Cells showing data Log<sub>2</sub>FC>1 and adjusted p<0.05\* are colour coded. Complementary Log<sub>2</sub>FC and TPM colour scale heatmaps are shown in Figure S9 in the Supplementary material.

*Nimodipine exerts complex action on microglial immune response, acting at multiple sites*

In our primary microglial monocultures, nimodipine administered with LPS altered the expression of 110 genes compared to LPS alone (Figs. 5-6). Of these DEGs, 29 were upregulated and 81 were downregulated. Remarkably, nimodipine had opposite effects to LPS (Fig. 6). Screening of these 110 genes revealed that at least 20 were associated with microglial immune response, 7 with cell adhesion, and 2 with autophagy regulation (Fig. 6, Table 2), in addition to 4 involved in intracellular Ca<sup>2+</sup> homeostasis shown above (Table 1). Downregulated DEGs involved in immune function included genes of toll-like receptor 9 (Tlr9) that was upregulated by LPS alone, in agreement with previous reports (Olson and Miller, 2004), and a negative feedback regulator of TLR signalling (Zc3h12d). The expression of cytokine receptors interleukin-6 receptor (Il6r) and a TNF receptor (Tnfrsf8) increased by LPS was also downregulated by nimodipine, along with the immune suppressor modulator fibrinogen-like protein 2 (Fgl2). Concerning the complement system, complement C1q (C1qc) and a complement receptor of complement fragment C3b (Vsig4) were downregulated by nimodipine opposing LPS effect. Finally, the expression of the MHC class II transactivator CIITA (Ciita) and CD36 (Cd36) also decreased at the presence of nimodipine. Upregulated DEGs associated with immune function were somatostatin 4 receptor (Sstr4), proposed to regulate microglial activation and phagocytosis (Sandoval et al., 2019; Silwal et al., 2022), and an  $\alpha$ -disintegrin and metalloproteinase with thrombospondin motifs (Adamts12) (Table 2; Fig. 6).

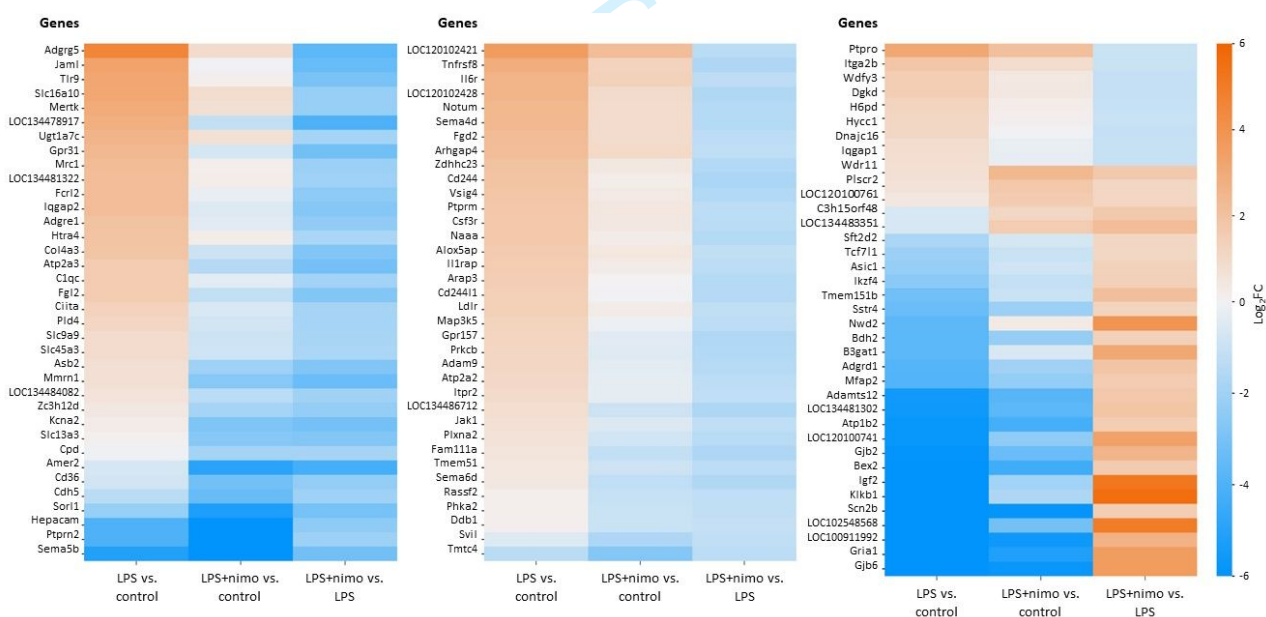


**Figure 6.** Heat maps of differentially expressed genes (DEGs) selected for significant change by nimodipine treatment (LPS+nimodipine) compared to LPS challenge alone (selection criteria:  $-1 > \text{Log}_2\text{FC} > 1$  and  $\text{adj.}p < 0.05$ ).

Among the DEGs associated with cell adhesion, a member of the junctional adhesion molecule transmembrane protein family (Jam1), an  $\alpha$ -disintegrin and metalloproteinase (Adam9), and an integrin cell adhesion receptor (Itga2b) were downregulated in nimodipine-treated cultures, counteracting LPS effect. In contrast, genes of gap junction proteins beta 2 and beta 6 (Gjb2 and Gjb6, respectively) were upregulated,

opposing LPS. Finally, genes of the autophagy regulators Wdfy3, which bridges cargo to the molecular machinery that builds autophagosomes (Filimonenko et al., 2010; Napoli et al., 2021), and Dnajc16, which determines the size of autophagosomes (Yamamoto et al., 2020), were downregulated by nimodipine, counteracting LPS effect (Table 2; Fig. 6).

**Table 2.** Selected differentially expressed genes (DEGs) by nimodipine treatment of primary microglia monocultures, grouped by function.

Function	Gene	Protein	LPS vs. Control	LPS+nimo vs. Control	nimo+LPS vs. LPS
Immune response	Tlr9	Toll Like Receptor 9	3.1561*	0.1871	-2.9690*
	Il6r	Il6 receptor	2.6244*	1.3293*	-1.2951*
	Fgd2	FGD2	2.2662*	0.9111*	-1.3551*
	Tnfrsf8	TNF Receptor Superfamily Member 8 (CD30)	2.9473*	1.2885*	-1.6588*
	Fcrl2	Fc Receptor Like 2	2.2251*	-0.2329	-2.4579*
	Cd244	CD244	1.9378*	0.1964	-1.7414*
	Vsig4	V-Set And Immunoglobulin Domain Containing 4	1.8700*	0.2840	-1.5861*
	Csf3r	Colony Stimulating Factor 3 Receptor	1.7708*	0.3918	-1.3790*
	Alox5ap	Arachidonate 5-Lipoxygenase Activating Protein	1.6148*	0.4358	-1.1789*
	Il1rap	Interleukin 1 Receptor Accessory Protein	1.5784*	0.2614	-1.3169*
	C1qc	Complement C1q C Chain	1.5763*	-0.3748	-1.9511*
	Fgl2	Fibrinogen-like protein 2	1.5614*	-1.1598	-2.7212*
	Cd244l1	CD244 molecule like 1	1.4525*	-0.0051	-1.4575*
	Ciita	class II, major histocompatibility complex, transactivator	1.2981*	-0.5630	-1.8612*
	Pld4	Phospholipase D Family Member 4	1.1346*	-0.7653*	-1.8999*
	Jak1	Janus Kinase 1	0.6950*	-0.5573*	-1.2523*
	Zc3h12d	Zinc Finger CCCH-Type Containing 12D	0.4047	-1.8988*	-2.3034*
	Cd36	platelet glycoprotein 4	-0.7784	-1.7757*	-2.3405*
Sstr4	Somatostatin Receptor 4	-3.3714*	-2.1223*	1.2491*	
Adams12	disintegrin and metalloproteinase with thrombospondin motifs 12	-5.5776*	-3.8356*	1.7420*	
Cell adhesion	Jaml	Junction Adhesion Molecule Like	3.3154*	-0.0721	-3.3875*
	Itga2b	Integrin Subunit Alpha 2b	1.8737*	0.8655*	-1.0082*
	Adam 9	ADAM Metallopeptidase Domain 9	1.1258*	-0.3609	-1.4866*
	Cdh5	Cadherin 5	-1.3695*	-3.3867*	-2.0172*
	Hepacam	Hepatic And Glial Cell Adhesion Molecule	-3.9963*	-6.4712*	-2.4749*
	Gjb2	Gap Junction Protein Beta 2	-5.9060*	-3.3409*	2.5651*
	Gjb6	Gap Junction Protein Beta 6	-9.3566*	-5.7405*	3.6161*
Auto-phagy	Wdfy3	WD Repeat And FYVE Domain Containing 3	1.5122*	0.4130	-1.0992*
	Dnajc16	DnaJ homolog subfamily C member 16	1.0805*	-0.0147	-1.0952*

Upregulated      Downregulated      No change

Change in mRNA expression is expressed as Log<sub>2</sub>FC (adjusted p<0.05\*); Cells showing data Log<sub>2</sub>FC>1 and adjusted p<0.05\* are colour coded. Complementary Log<sub>2</sub>FC and TPM colour scale heatmaps are shown in Figure S10 in the Supplementary material.

Finally, functional enrichment analysis confirmed the positive effect of nimodipine on intercellular connections (e.g., connexin complex, gap junction, intercellular transport), and elucidated the negative effect on the activity of several enzymes implicated in intracellular signal transduction (e.g., kinases and transferases), in addition to Ca<sup>2+</sup> trafficking of the ER (Fig. 7).

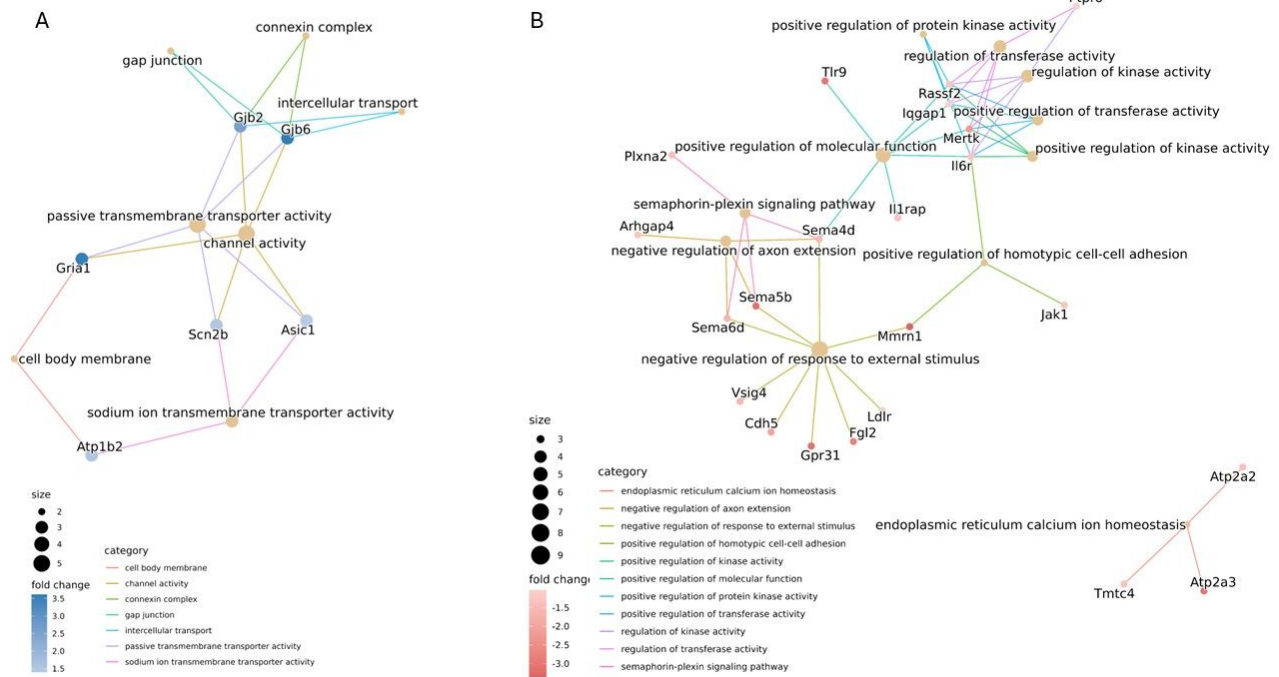


**Figure 7.** Functional enrichment analysis results are displayed in gene-concept network plots (cnet plots) to illustrate the effect of nimodipine on biological processes (BP). Upregulated (A) and downregulated (B) functions are shown by linkages of genes and gene ontology (GO) terms (LPS+nimodipine vs. LPS alone).

## Discussion

In this study, exposing live brain slice preparations to mOGD or challenging microglial cultures with LPS caused microglial activation, which was clearly indicated by a shift toward amoeboid morphology (Figs. 1-2), and, in cell cultures, by increased phagocytosis (Fig. 4). The shift in microglial phenotype was underscored by complex changes in gene activity expression (Fig. 5). Importantly, the addition of nimodipine to the activated brain slice preparations and microglial cultures suppressed microglial activation (Figs. 1-4), caused change in the expression of a distinct group of genes associated with immune response (Figs. 5-6, Tables 2-3), and thus delivered two main messages. First,  $\text{Ca}^{2+}$  influx through LVGCCs plays an important role in microglial activation, by modulating gene expression. Second, the LVGCC blocker nimodipine confers partial mitigation against microglial activation by modulating distinct elements of the immune response, and may offer benefit as an anti-neuroinflammatory agent.

There is a consensus that microglial activation is associated with increased intracellular  $\text{Ca}^{2+}$  concentration in response to a variety of danger signals (Hopp et al., 2020), including the widely used activator LPS (Hoffmann et al., 2003). Less is known about which pathways of  $\text{Ca}^{2+}$  movement are involved and how an inflammatory stimulus redirects transmembrane microglial  $\text{Ca}^{2+}$  currents. Here we show that the expression of the purinergic P2X4 receptors and TRPM2 channels was upregulated by LPS, suggesting that these two pathways may be the predominant  $\text{Ca}^{2+}$  influx pathways during microglial activation. Consistent with our data, the microglial P2X4

1  
2  
3 receptors activated by elevated extracellular ATP concentrations open to allow  $\text{Ca}^{2+}$  influx and initiate an  
4 inflammatory response (Suurväli et al., 2017), and are upregulated in various brain and spinal cord pathologies  
5 involving neuroinflammation (Montilla et al., 2020). Similarly, LPS/IFN $\gamma$  stimulation of microglia induces  
6 TRPM2-mediated  $\text{Ca}^{2+}$  signalling (Miyake et al., 2014), and TRPM2 channels emerge as part of a feedback loop  
7 that promotes pro-inflammatory polarization (Raghunatha et al., 2020). In contrast, we found that the  
8 expression of VGCCs and glutamate-gated cation channels was downregulated in response to LPS, implying  
9 reduced  $\text{Ca}^{2+}$  conductance through these channels, which may be compensative. Our data are consistent with  
10 those showing that cultured microglia express the Cav1.2 and Cav1.3 proteins of LVGCCs (Espinosa-Parrilla et  
11 al., 2015). However, we did not observe an upregulation of these genes, in contrast to the increased Cav1.2  
12 protein levels quantified earlier by Western blotting, after LPS/TRP stimulation of BV2 microglia (Espinosa-  
13 Parrilla et al., 2015). The discrepancy in the results may be due to the different model systems (primary  
14 microglial cultures versus an immortalized cell line) or post-translational modification of Cav proteins  
15 (Szymanowicz et al., 2024). Importantly, although *Cacna1c* and *Cacna1d* gene expression was reduced by LPS  
16 in our preparations (Table 1), our results imply that the LVGCC proteins Cav1.2 and Cav1.3 (encoded by  
17 *Cacna1c* and *Cacna1d*, respectively) must have been abundant enough in the plasmalemma to mediate  $\text{Ca}^{2+}$   
18 influx relevant to microglial activation and to serve as the target of nimodipine to produce the observed  
19 effects.  
20  
21  
22  
23  
24  
25  
26  
27  
28  
29  
30  
31

32 In addition to the lower expression of the above mentioned plasmalemmal  $\text{Ca}^{2+}$  channels,  $\text{Ca}^{2+}$  release  
33 from the ER must also have been inhibited during activation, as evidenced by the downregulation of several  
34 ryanodine and IP3 receptor genes. At the same time, active  $\text{Ca}^{2+}$  transport into the ER appeared to be  
35 augmented by the upregulation of SERCA genes (*Atp2a2* and *Atp2a3*), in agreement with recent findings  
36 focusing on SERCA2b (Morales-Ropero et al., 2021). These changes suggest that  $\text{Ca}^{2+}$  storage in the ER is  
37 favoured during microglial activation, presumably to counterbalance the intracellular  $\text{Ca}^{2+}$  load through  
38 membrane channels in response to the inflammatory stimulus. This concept seems to be supported by the  
39 observation that the SERCA genes were downregulated when nimodipine, a  $\text{Ca}^{2+}$  channel blocker was added  
40 to our preparations (Table 1). Nimodipine must have reduced the overall  $\text{Ca}^{2+}$  influx through the plasmalemma  
41 (*Silei et al., 1999; Hegg et al., 2000*), hence the SERCA genes were not suppressed. Incidentally, SERCA  
42 inhibition was previously found to reduce microglial phagocytosis (Morales-Ropero et al., 2021), which is  
43 consistent with our data showing that nimodipine inhibited phagocytic activity (Fig. 4) concomitant with the  
44 downregulation of SERCA genes (Table 1).  
45  
46  
47  
48  
49  
50  
51  
52  
53

54 Nimodipine consistently inhibited the phenotypic shift of microglia in activated brain slice preparations  
55 and cultures, suggesting that microglia were reliably targeted by the treatment in their neural tissue  
56 environment, in co-culture with neurons and astrocytes, and in monoculture (Figs. 1-4). We explored DEGs  
57 underlying these microglial morphological and functional phenotypic changes and provide a novel,  
58  
59  
60

1  
2  
3 comprehensive overview of nimodipine action at the level of gene expression in activated primary microglial  
4 cultures (Fig. 6, Table 2). Nimodipine is assumed to have achieved its effects on gene expression primarily by  
5 modulating intracellular  $\text{Ca}^{2+}$  signalling (Barbado et al., 2009), taken that  $\text{Ca}^{2+}$  is a well-known second  
6 messenger in the control of gene expression. At least three  $\text{Ca}^{2+}$ -dependent gene transcriptional pathways  
7 regulated by VGCCs have been previously identified, including (i) a calmodulin-dependent kinase and cAMP  
8 response element binding protein (CREB)-dependent pathway, (ii) a pathway initiated by  $\text{Ca}^{2+}$ -sensitive  
9 proteins, associated with the VGCC signalling complex, that activate transcription factors, and (iii) a pathway  
10 regulated by  $\text{Ca}^{2+}$ -binding transcription factors (e.g., DREAM) (Barbado et al., 2009). In addition, a proteolytic  
11 fragment of the intracellular carboxyl terminus of the  $\alpha$  subunit of LVGCCs (specifically of Cav1.2 and Cav 1.3  
12 found here on microglia) can translocate to the cell nucleus to act as a transcription factor itself (Gomez-  
13 Ospina et al., 2006; Lu et al., 2015). As evidenced by our functional enrichment analysis (Fig. 7B), nimodipine  
14 is thought to finely modulate intracellular signal transduction pathways (e.g., expression of protein kinases),  
15 by inhibiting LVGCC opening to cause the gene expression changes described here.

16  
17 Although the widely accepted action of nimodipine is blockade of LVGCCs, a limitation to the  
18 interpretation of our results is that dihydropyridine  $\text{Ca}^{2+}$  channel blockers may target alternative cellular sites,  
19 including Kv1.3 voltage-gated potassium channels (Kazama et al., 2013), mineralocorticoid receptors (Dietz,  
20 Du et al., 2008), or CFTR chloride channels (Pedemonte et al., 2005). The transcript in our experiments included  
21 Kcna3 and Nr3c2 (the mRNA encoding Kv1.3 and mineralocorticoid receptors, respectively), but not Cftr.  
22 Therefore, the possibility that suppressed activation of Kv1.3 and mineralocorticoid receptors contribute to  
23 the effect of nimodipine cannot be excluded.

24  
25 **The concentration of nimodipine used may be considered as a limitation to the translational value of these**  
26 **results. The plasma or serum concentration of nimodipine after intravenous infusion is one order of magnitude**  
27 **lower, in the ng/ml range, compared to the dose used here (Koskimäki et al., 2016; Albanna et al., 2017). The**  
28 **currently used clinical dose may not provide the full therapeutic benefit of nimodipine, as the administered**  
29 **concentration of nimodipine in patients is limited by side effects such as systemic hypotension (Ahmed et al.,**  
30 **2000) or cerebrovascular steal (Kecskés et al., 2023). To circumvent this problem and increase therapeutic**  
31 **benefit, novel drug delivery approaches using microparticles and nanoparticles have been explored to deliver**  
32 **high concentrations of nimodipine locally to the site of cerebral injury to achieve higher efficacy with low risk**  
33 **of systemic side effects (Hänggi et al., 2008; Tóth et al., 2020). This ongoing work on targeted drug delivery**  
34 **and the experimental approach presented here are thought to be complementary and synergistic.**

35  
36 In conclusion, this study has provided evidence that nimodipine effectively suppresses microglial  
37 activation by modulating  $\text{Ca}^{2+}$ -dependent intracellular signalling cascades and gene expression involved in  
38 microglial  $\text{Ca}^{2+}$  homeostasis and immune responses. On the basis of these novel findings, consideration should  
39  
40  
41  
42  
43  
44  
45  
46  
47  
48  
49  
50  
51  
52  
53  
54  
55  
56  
57  
58  
59  
60

1  
2  
3 be given to expanding the medical field of indication of nimodipine to be used to attenuate neuroinflammation  
4 in acute brain injury or chronic neurodegeneration.  
5  
6  
7

### 8 **Data Availability**

9  
10 The RNA sequencing data generated in this study have been deposited in the NCBI Sequence Read Archive  
11 (SRA) under the BioProject accession number PRJNA1185105. The scripts utilized to analyse the data and to  
12 generate the images are available upon request from the corresponding author.  
13  
14  
15

### 16 **Funding**

17  
18 The author(s) disclosed receipt of the following financial support for the research: The EU's Horizon 2020  
19 research and innovation program grant number 739593; the National Research, Development and Innovation  
20 Office of Hungary (grant numbers K134334, K146725, FK142218 and 2023-1.1.1-PIACI\_FÓKUSZ-2024-00029);  
21 the Ministry of Innovation and Technology of Hungary and the National Research, Development and  
22 Innovation Fund (grant number TKP2021-EGA-28 financed under the TKP2021-EGA funding scheme); the  
23 Ministry of Culture and Innovation of Hungary (grant number EKÖP-24-4-SZTE-622); the National Brain  
24 Research Program 3.0 of the Hungarian Academy of Sciences; the Research Fund of the Albert Szent-Györgyi  
25 Medical School, University of Szeged, Hungary; and the University of Szeged Open Access Fund (Nr. 7516).  
26 Project no. RRF-2.3.1-21-2022-00015 has been implemented with the support provided by the European  
27 Union.  
28  
29  
30  
31  
32  
33  
34  
35  
36

### 37 **Competing interests**

38 The authors declare that they have no competing interests.  
39  
40  
41

### 42 **Authors' contributions**

43 I. P.: Formal Analysis, Investigation, Visualization, Writing – original draft; V.V.: Formal Analysis,  
44 Visualization; E.Q.: Formal Analysis, Visualization, Writing – review & editing; R.F.: Formal Analysis,  
45 Investigation, Visualization; D. K.: Formal Analysis; Investigation; K.V.: Formal Analysis, Visualization; P.A.S.:  
46 Formal Analysis; Á. M.: Methodology, Supervision, Writing – review & editing; K.G.: Supervision, Writing –  
47 review & editing; F. B.: Supervision, Writing – review & editing, Funding acquisition; E. F.: Conceptualization,  
48 Formal Analysis, Visualization, Supervision, Writing – original draft, Funding acquisition.  
49  
50  
51  
52  
53  
54  
55  
56  
57  
58  
59  
60

## References

- Ahmed, N., Näsman, P., Wahlgren, N.G. (2000). Effect of intravenous nimodipine on blood pressure and outcome after acute stroke. *Stroke*, *31*(6), 1250-5. doi: 10.1161/01.str.31.6.1250.
- Albanna, W., Weiss, M., Conzen, C., Clusmann, H., Schneider, T., Reinsch, M., Müller, M., Wiesmann, M., Höllig, A., Schubert, G.A. (2017). Systemic and Cerebral Concentration of Nimodipine During Established and Experimental Vasospasm Treatment. *World Neurosurgery*, *102*, 459-465. doi: 10.1016/j.wneu.2017.03.062.
- Allen, G.S., Ahn, H.S., Preziosi, T.J., Battye, R., Boone, S.C., Boone, S.C., Chou, S.N., Kelly, D.L., Weir, B.K., Crabbe, R.A., Lavik, P.J., Rosenbloom, S.B., Dorsey, F.C., Ingram, C.R., Mellits, D.E., Bertsch, L.A., Boisvert, D.P., Hundley, M.B., Johnson, R.K., Strom, J.A., & Transou, C.R. (1983). Cerebral arterial spasm--a controlled trial of nimodipine in patients with subarachnoid hemorrhage. *The New England Journal of Medicine*, *308*(11), 619-24. <https://doi.org/10.1056/NEJM198303173081103>.
- Andrews, S. (2010). FastQC: a quality control tool for high throughput sequence data. Available online at: <http://www.bioinformatics.babraham.ac.uk/projects/fastqc>
- Barbado, M., Fablet, K., Ronjat, M., & De Waard, M. (2009). Gene regulation by voltage-dependent calcium channels. *Biochimica et Biophysica Acta*, *1793*(6), 1096-104. <https://doi.org/10.1016/j.bbamcr.2009.02.004>.
- Carlson, A.P., Hänggi, D., Macdonald, R.L., & Shuttleworth, C.W. (2020). Nimodipine Reappraised: An Old Drug With a Future. *Current Neuropharmacology*, *18*(1), 65-82. <https://doi.org/10.2174/1570159X17666190927113021>.
- Chen, S., Zhou, Y., Chen, Y., & Gu, J. (2018). Fastp: An ultra-fast all-in-one FASTQ preprocessor. In: *Bioinformatics*, *34*, <https://doi.org/10.1093/bioinformatics/bty560>
- Chen, Y., Chu, J.M.T., Chang, R.C.C., & Wong, G.T.C. (2022). The Complement System in the Central Nervous System: From Neurodevelopment to Neurodegeneration. *Biomolecules*, *12*(2), 337. <https://doi.org/10.3390/biom12020337>.
- Colton, C.A., Jia, M., Li, M.X., & Gilbert, D.L. (1994). K<sup>+</sup> modulation of microglial superoxide production: involvement of voltage-gated Ca<sup>2+</sup> channels. *American Journal of Physiology*, *266*(6 Pt 1), C1650-5. <https://doi.org/10.1152/ajpcell.1994.266.6.C1650>.
- Curtis, M.J., Alexander, S.P.H., Cirino, G., George, C.H., Kendall, D.A., Insel, P.A., Izzo, A.A., Ji, Y., Panettieri, R.A., Patel, H.H., Sobey, C.G., Stanford, S.C., Stanley, P., Stefanska, B., Stephens, G.J., Teixeira, M.M., Vergnolle, N., & Ahluwalia, A. (2022). Planning experiments: Updated guidance on experimental design and analysis and their reporting III. *British Journal of Pharmacology*, *179*(15), 3907-3913. <https://doi.org/10.1111/bph.15868>.
- Dietz, J.D., Du, S., Bolten, C.W., Payne, M.A., Xia, C., Blinn, J.R., Funder, J.W., & Hu, X. (2008). A number of marketed dihydropyridine calcium channel blockers have mineralocorticoid receptor antagonist activity. *Hypertension*, *51*(3), 742-8. <https://doi.org/10.1161/HYPERTENSIONAHA.107.103580>.
- Dietz, R.M., Weiss, J.H., & Shuttleworth, C.W. (2008). Zn<sup>2+</sup> influx is critical for some forms of spreading depression in brain slices. *Journal of Neuroscience*, *28*(32), 8014-24. <https://doi.org/10.1523/JNEUROSCI.0765-08.2008>.

1  
2  
3 Dobin, A., Davis, C.A., Schlesinger, F., Drenkow, J., Zaleski, C., Jha, S., Batut, P., Chaisson, M., & Gingeras, T.R.  
4 (2013). STAR: ultrafast universal RNA-seq aligner. *Bioinformatics*, 29(1), 15-21.  
5 <https://doi.org/10.1093/bioinformatics/bts635>.

6  
7 Eichhoff, G., Brawek, B., & Garaschuk, O. (2011). Microglial calcium signal acts as a rapid sensor of single  
8 neuron damage in vivo. *Biochimica et Biophysica Acta*, 1813(5), 1014-24.  
9 <https://doi.org/10.1016/j.bbamcr.2010.10.018>.

10  
11 Espinosa-Parrilla, J.F., Martínez-Moreno, M., Gasull, X., Mahy, N., & Rodríguez, M.J. (2015). The L-type voltage-  
12 gated calcium channel modulates microglial pro-inflammatory activity. *Molecular and Cellular Neuroscience*,  
13 64, 104-15. <https://doi.org/10.1016/j.mcn.2014.12.004>.

14  
15 Feigin, V.L., Rinkel, G.J., Algra, A., Vermeulen, M., & van Gijn, J. (1998). Calcium antagonists in patients with  
16 aneurysmal subarachnoid hemorrhage: a systematic review. *Neurology*, 50(4), 876-83.  
17 <https://doi.org/10.1212/wnl.50.4.876>.

18  
19 Filimonenko, M., Isakson, P., Finley, K.D., Anderson, M., Jeong, H., Melia, T.J., Bartlett, B.J., Myers, K.M.,  
20 Birkeland, H.C., Lamark, T., Krainc, D., Brech, A., Stenmark, H., Simonsen, A., & Yamamoto, A. (2010). The  
21 selective macroautophagic degradation of aggregated proteins requires the PI3P-binding protein Alfy.  
22 *Molecular Cell*, 38(2), 265-79. <https://doi.org/10.1016/j.molcel.2010.04.007>.

23  
24 Frank, R., Szarvas, P.A., Pesti, I., Zsigmond, A., Berkecz, R., Menyhárt, Á., Bari, F., & Farkas, E. (2024).  
25 Nimodipine inhibits spreading depolarization, ischemic injury, and neuroinflammation in mouse live brain slice  
26 preparations. *European Journal of Pharmacology*, 977, 176718.  
27 <https://doi.org/10.1016/j.ejphar.2024.176718>.

28  
29 Gomez-Ospina, N., Tsuruta, F., Barreto-Chang, O., Hu, L., & Dolmetsch, R. (2006). The C terminus of the L-type  
30 voltage-gated calcium channel Ca(V)1.2 encodes a transcription factor. *Cell*, 127(3), 591-606.  
31 <https://doi.org/10.1016/j.cell.2006.10.017>.

32  
33 Hänggi, D., Beseoglu, K., Turowski, B., Steiger, H.J. (2008) Feasibility and safety of intrathecal nimodipine on  
34 posthaemorrhagic cerebral vasospasm refractory to medical and endovascular therapy. *Clinical Neurology and*  
35 *Neurosurgery*, 110(8), 784-90. doi: 10.1016/j.clineuro.2008.05.001.

36  
37 Hegg, C.C., Hu, S., Peterson, P.K., & Thayer, S.A. (2000). Beta-chemokines and human immunodeficiency virus  
38 type-1 proteins evoke intracellular calcium increases in human microglia. *Neuroscience*, 98(1), 191-9.  
39 [https://doi.org/10.1016/s0306-4522\(00\)00101-9](https://doi.org/10.1016/s0306-4522(00)00101-9).

40  
41 Hoffmann, A., Kann, O., Ohlemeyer, C., Hanisch, U.K., & Kettenmann, H. (2003). Elevation of basal intracellular  
42 calcium as a central element in the activation of brain macrophages (microglia): suppression of receptor-  
43 evoked calcium signaling and control of release function. *Journal of Neuroscience*, 23(11), 4410-9.  
44 <https://doi.org/10.1523/JNEUROSCI.23-11-04410.2003>.

45  
46 Hopp, S.C. (2021). Targeting microglia L-type voltage-dependent calcium channels for the treatment of central  
47 nervous system disorders. *Journal of Neuroscience Research*, 99(1), 141-162.  
48 <https://doi.org/10.1002/jnr.24585>.

49  
50 Huang, H., Yu, D., & Soong, T.W. (2013). C-terminal alternative splicing of CaV1.3 channels distinctively  
51 modulates their dihydropyridine sensitivity. *Molecular Pharmacology*, 84(4), 643-53.  
52 <https://doi.org/10.1124/mol.113.087155>.

1  
2  
3 Jin, M.M., Wang, F., Qi, D., Liu, W.W., Gu, C., Mao, C.J., Yang, Y.P., Zhao, Z., Hu, L.F., & Liu, C.F. (2018). A Critical  
4 Role of Autophagy in Regulating Microglia Polarization in Neurodegeneration. *Frontiers in Aging*  
5 *Neuroscience*, *10*, 378. <https://doi.org/10.3389/fnagi.2018.00378>.

7  
8 Jurga, A.M., Paleczna, M., & Kuter, K.Z. (2020). Overview of General and Discriminating Markers of Differential  
9 Microglia Phenotypes. *Frontiers in Cellular Neuroscience*, *14*, 198. <https://doi.org/10.3389/fncel.2020.00198>.  
10 eCollection 2020.

11  
12 Kata, D., Földesi, I., Feher, L.Z., Hackler, L. Jr., Puskas, L.G., & Gulya, K. (2016). Rosuvastatin enhances anti-  
13 inflammatory and inhibits pro-inflammatory functions in cultured microglial cells. *Neuroscience*, *314*, 47-63.  
14 <https://doi.org/10.1016/j.neuroscience.2015.11.053>.

15  
16 Kazama, I., Maruyama, Y., & Matsubara, M. (2013). Benidipine persistently inhibits delayed rectifier K(+)-  
17 channel currents in murine thymocytes. *Immunopharmacology and Immunotoxicology*, *35*(1), 28-33.  
18 <https://doi.org/10.3109/08923973.2012.723011>.

19  
20 Kazda, S., & Towart, R. (1982). Nimodipine: a new calcium antagonistic drug with a preferential  
21 cerebrovascular action. *Acta Neurochirurgica (Wien)*, *63*(1-4), 259-65. <https://doi.org/10.1007/BF01728880>.

22  
23  
24 **Kecskés, S., Menyhárt, Á., Bari, F., Farkas, E. (2023). Nimodipine augments cerebrovascular reactivity in aging**  
25 **but runs the risk of local perfusion reduction in acute cerebral ischemia. *Frontiers in Aging Neuroscience*, *15*,**  
26 **1175281. doi: 10.3389/fnagi.2023.1175281.**

27  
28  
29 Kilkeny, C., Browne, W., Cuthill, I.C., Emerson, M., & Altman, D.G. (2010). NC3Rs Reporting Guidelines  
30 Working Group. Animal research: reporting in vivo experiments: the ARRIVE guidelines. *British Journal of*  
31 *Pharmacology*, *160*(7), 1577-9. <https://doi.org/10.1111/j.1476-5381.2010.00872.x>.

32  
33 **Koskimäki, J., Tarkia, M., Ahtola-Sättilä, T., Saloranta, L., Laakso, A., Frantzen, J. (2016). Absorption, elimination**  
34 **and cerebrospinal fluid concentrations of nimodipine in healthy beagle dogs receiving human intravenous and**  
35 **oral formulation. *European Journal of Drug Metabolism and Pharmacokinetics*, *41*(3), 295-300. doi:**  
36 **10.1007/s13318-015-0258-5.**

37  
38  
39 Law, C.W., Chen, Y., Shi, W., & Smyth, G.K. (2014). voom: Precision weights unlock linear model analysis tools  
40 for RNA-seq read counts. *Genome Biology*, *15*(2), R29. <https://doi.org/10.1186/gb-2014-15-2-r29>.

41  
42  
43 Lehnardt, S., Massillon, L., Follett, P., Jensen, F.E., Ratan, R., Rosenberg, P.A., Volpe, J.J., & Vartanian, T. (2003).  
44 Activation of innate immunity in the CNS triggers neurodegeneration through a Toll-like receptor 4-dependent  
45 pathway. *Proceedings of the National Academy of Sciences of the United States of America*, *100*(14), 8514-9.  
46 <https://doi.org/10.1073/pnas.1432609100>.

47  
48  
49 Li, Y., Hu, X., Liu, Y., Bao, Y., & An, L. (2009). Nimodipine protects dopaminergic neurons against inflammation-  
50 mediated degeneration through inhibition of microglial activation. *Neuropharmacology*, *56*(3), 580-9.  
51 <https://doi.org/10.1016/j.neuropharm.2008.10.016>.

52  
53  
54 Liao, Y., Smyth, G.K., & Shi, W. (2014). featureCounts: an efficient general purpose program for assigning  
55 sequence reads to genomic features. *Bioinformatics*, *30*(7), 923-30.  
56 <https://doi.org/10.1093/bioinformatics/btt656>.

57  
58  
59 Liu, L., Kearns, K.N., Eli, I., Sharifi, K.A., Soldozy, S., Carlson, E.W., Scott, K.W., Sluzewski, M.F., Acton, S.T.,  
60 Stauderman, K.A., Kalani, M.Y.S., Park, M., & Tvrđik, P. (2021). Microglial Calcium Waves During the  
Hyperacute Phase of Ischemic Stroke. *Stroke*, *52*(1), 274-283.  
<https://doi.org/10.1161/STROKEAHA.120.032766>.

- 1  
2  
3 Lowry, O.H., Rosenbrough, N.J., Farr, A.L., & Randall, R.J. (1951). Protein measurement with the Folin phenol  
4 reagent. *Journal of Biological Chemistry*, *193*(1), 265-75. PMID: 14907713.  
5  
6 Lu, L., Sirish, P., Zhang, Z., Woltz, R.L., Li, N., Timofeyev, V., Knowlton, A.A., Zhang, X.D., Yamoah, E.N., &  
7 Chiamvimonvat, N. (2015). Regulation of gene transcription by voltage-gated L-type calcium channel, Cav1.3.  
8 *Journal of Biological Chemistry*, *290*(8), 4663-76. <https://doi.org/10.1074/jbc.M114.586883>.  
9  
10 Menyhárt, Á., Bálint, A.R., Kozák, P., Bari, F., & Farkas, E. (2024). Nimodipine accelerates the restoration of  
11 functional hyperemia during spreading oligemia. *Journal of Neurochemistry*, *168*(5), 888-898.  
12 <https://doi.org/10.1111/jnc.15792>.  
13  
14 Menyhárt, Á., Farkas, A.E., Varga, D.P., Frank, R., Tóth, R., Bálint, A.R., Makra, P., Dreier, J.P., Bari, F., Krizbai,  
15 I.A., & Farkas, E. (2018). Large-conductance Ca<sup>2+</sup>-activated potassium channels are potently involved in the  
16 inverse neurovascular response to spreading depolarization. *Neurobiology of Disease*, *119*, 41-52.  
17 <https://doi.org/10.1016/j.nbd.2018.07.026>. Epub 2018 Jul 24.  
18  
19 Miyake, T., Shirakawa, H., Kusano, A., Sakimoto, S., Konno, M., Nakagawa, T., Mori, Y., & Kaneko, S. (2014).  
20 TRPM2 contributes to LPS/IFN $\gamma$ -induced production of nitric oxide via the p38/JNK pathway in microglia.  
21 *Biochemical and Biophysical Research Communications*, *444*(2), 212-7.  
22 <https://doi.org/10.1016/j.bbrc.2014.01.022>.  
23  
24 Montilla, A., Mata, G.P., Matute, C., & Domercq, M. (2020). Contribution of P2X4 Receptors to CNS Function  
25 and Pathophysiology. *International Journal of Molecular Sciences*, *21*(15), 5562.  
26 <https://doi.org/10.3390/ijms21155562>.  
27  
28 Morales-Ropero, J.M., Arroyo-Urea, S., Neubrand, V.E., Martín-Oliva, D., Marín-Teva, J.L., Cuadros, M.A.,  
29 Vangheluwe, P., Navascués, J., Mata, A.M., & Sepúlveda, M.R. (2021). The endoplasmic reticulum Ca<sup>2+</sup> -  
30 ATPase SERCA2b is upregulated in activated microglia and its inhibition causes opposite effects on migration  
31 and phagocytosis. *Glia*, *69*(4), 842-857. <https://doi.org/10.1002/glia.23931>.  
32  
33 Napoli, E., Panoutsopoulos, A.A., Kysar, P., Satriya, N., Sterling, K., Shibata, B., Imai, D., Ruskin, D.N., Zarbalis,  
34 K.S., & Giulivi, C. (2021). Wdfy3 regulates glycophyagy, mitophagy, and synaptic plasticity. *Journal of Cerebral*  
35 *Blood Flow and Metabolism*, *41*(12), 3213-3231. <https://doi.org/10.1177/0271678X211027384>.  
36  
37 Olson, J.K., & Miller, S.D. (2004). Microglia initiate central nervous system innate and adaptive immune  
38 responses through multiple TLRs. *The Journal of Immunology*, *173*(6), 3916-24.  
39 <https://doi.org/10.4049/jimmunol.173.6.3916>.  
40  
41 Pedemonte, N., Diena, T., Caci, E., Nieddu, E., Mazzei, M., Ravazzolo, R., Zegarra-Moran, O., & Galletta, L.J.  
42 (2005). Antihypertensive 1,4-dihydropyridines as correctors of the cystic fibrosis transmembrane conductance  
43 regulator channel gating defect caused by cystic fibrosis mutations. *Molecular Pharmacology*, *68*(6), 1736-46.  
44 <https://doi.org/10.1124/mol.105.015149>.  
45  
46 Pesti, I., Légrádi, Á., & Farkas, E. (2024). Primary microglia cell cultures in translational research: Strengths and  
47 limitations. *Journal of Biotechnology*, *386*, 10-18. <https://doi.org/10.1016/j.jbiotec.2024.03.005>.  
48  
49 Podleśny-Drabiniok, A., Marcora, E., & Goate, A.M. (2020). Microglial Phagocytosis: A Disease-Associated  
50 Process Emerging from Alzheimer's Disease Genetics. *Trends in Neurosciences*, *43*(12), 965-979.  
51 <https://doi.org/10.1016/j.tins.2020.10.002>.  
52  
53 Pulido-Salgado, M., Vidal-Taboada, J.M., Barriga, G.G., Solà, C., & Saura, J. (2018). RNA-Seq transcriptomic  
54 profiling of primary murine microglia treated with LPS or LPS + IFN $\gamma$ . *Scientific Reports*, *8*(1), 16096.  
55 <https://doi.org/10.1038/s41598-018-34412-9>.  
56  
57  
58  
59  
60

1  
2  
3 Raghunatha, P., Vosoughi, A., Kauppinen, T.M., & Jackson, M.F. (2020). Microglial NMDA receptors drive pro-  
4 inflammatory responses via PARP-1/TRMP2 signaling. *Glia*, *68*(7), 1421-1434.  
5 <https://doi.org/10.1002/glia.23790>.

6  
7 Robinson, M.D., McCarthy, D.J., & Smyth, G.K. (2010). edgeR: a Bioconductor package for differential  
8 expression analysis of digital gene expression data. *Bioinformatics*, *26*(1), 139-40.  
9 <https://doi.org/10.1093/bioinformatics/btp616>.

10  
11 Sabogal-Guáqueta, A.M., Marmolejo-Garza, A., Trombetta-Lima, M., Oun, A., Hunneman, J., Chen, T.,  
12 Koistinaho, J., Lehtonen, S., Kortholt, A., Wolters, J.C., Bakker, B.M., Eggen, B.J.L., Boddeke, E., & Dolga, A.  
13 (2023). Species-specific metabolic reprogramming in human and mouse microglia during inflammatory  
14 pathway induction. *Nature Communications*, *14*(1), 6454. <https://doi.org/10.1038/s41467-023-42096-7>.

15  
16 Sandoval, K., Umbaugh, D., House, A., Crider, A., & Witt, K. (2019). Somatostatin Receptor Subtype-4 Regulates  
17 mRNA Expression of Amyloid-Beta Degrading Enzymes and Microglia Mediators of Phagocytosis in Brains of  
18 3xTg-AD Mice. *Neurochemical Research*, *44*(11), 2670-80. <https://doi.org/10.1007/s11064-019-02890-6>.

19  
20 Silei, V., Fabrizi, C., Venturini, G., Salmons, M., Bugiani, O., Tagliavini, F., & Lauro, G.M. (1999). Activation of  
21 microglial cells by PrP and beta-amyloid fragments raises intracellular calcium through L-type voltage sensitive  
22 calcium channels. *Brain Research*, *818*(1), 168-70. [https://doi.org/10.1016/s0006-8993\(98\)01272-4](https://doi.org/10.1016/s0006-8993(98)01272-4).

23  
24 Silwal, A., House, A., Sandoval, K., Vijeth, S., Umbaugh, D., Crider, A., Mobayen, S., Neumann, W., & Witt, K.A.  
25 (2022). Novel Somatostatin Receptor-4 Agonist SM-I-26 Mitigates Lipopolysaccharide-Induced Inflammatory  
26 Gene Expression in Microglia. *Neurochemical Research*, *47*(3), 768-780. [https://doi.org/10.1007/s11064-021-](https://doi.org/10.1007/s11064-021-03482-z)  
27 03482-z.

28  
29 Suurväli, J., Boudinot, P., Kanellopoulos, J., & Rüütel Boudinot, S. (2017). P2X4: A fast and sensitive purinergic  
30 receptor. *Biomedical Journal*, *40*(5), 245-256. <https://doi.org/10.1016/j.bj.2017.06.010>.

31  
32 Szabó, Í., M. Tóth, O., Török, Z., Varga, D.P., Menyhárt, Á., Frank, R., Hantosi, D., Hunya, Á., Bari, F., Horváth,  
33 I., Vigh, L., & Farkas, E. (2019). The impact of dihydropyridine derivatives on the cerebral blood flow response  
34 to somatosensory stimulation and spreading depolarization. *British Journal of Pharmacology*, *176*(9), 1222-  
35 1234. <https://doi.org/10.1111/bph.14611>.

36  
37 Szabo, M., & Gulya, K. (2013). Development of the microglial phenotype in culture. *Neuroscience*, *241*, 280-  
38 95. <https://doi.org/10.1016/j.neuroscience.2013.03.033>.

39  
40 Szymanowicz, O., Drużdż, A., Słowikowski, B., Pawlak, S., Potocka, E., Goutor, U., Konieczny, M., Ciastoń, M.,  
41 Lewandowska, A., Jagodziński, P.P., Kozubski, W., & Dorszewska, J. (2024). A Review of the CACNA Gene  
42 Family: Its Role in Neurological Disorders. *Diseases*, *12*(5), 90. <https://doi.org/10.3390/diseases12050090>.

43  
44 Tang, L., Gamal El-Din, T.M., Swanson, T.M., Pryde, D.C., Scheuer, T., Zheng, N., & Catterall, W.A. (2016).  
45 Structural basis for inhibition of a voltage-gated Ca<sup>2+</sup> channel by Ca<sup>2+</sup> antagonist drugs. *Nature*, *537*(7618),  
46 117-121. <https://doi.org/10.1038/nature19102>.

47  
48 Thomas, A.L., Lehn, M.A., Janssen, E.M., Hildeman, D.A., & Chougnnet, C.A. (2022). Naturally-aged microglia  
49 exhibit phagocytic dysfunction accompanied by gene expression changes reflective of underlying neurologic  
50 disease. *Scientific Reports*, *12*(1), 19471. <https://doi.org/10.1038/s41598-022-21920-y>.

51  
52 Tóth, O.M., Menyhárt, Á., Varga, V.É., Hantosi, D., Ivánkovits-Kiss, O., Varga, D.P., Szabó, Í., Janovák, L., Dékány,  
53 I., Farkas, E., Bari, F. (2020). Chitosan nanoparticles release nimodipine in response to tissue acidosis to  
54 attenuate spreading depolarization evoked during forebrain ischemia. *Neuropharmacology*, *162*, 107850. doi:  
55 [10.1016/j.neuropharm.2019.107850](https://doi.org/10.1016/j.neuropharm.2019.107850).

1  
2  
3 Xu, W., & Lipscombe, D. (2001). Neuronal Ca(V)1.3alpha(1) L-type channels activate at relatively  
4 hyperpolarized membrane potentials and are incompletely inhibited by dihydropyridines. *Journal of*  
5 *Neuroscience*, 21(16), 5944-51. <https://doi.org/10.1523/JNEUROSCI.21-16-05944.2001>.  
6

7  
8 Yamamoto, Y.H., Kasai, A., Omori, H., Takino, T., Sugihara, M., Umemoto, T., Hamasaki, M., Hatta, T., Natsume,  
9 T., Morimoto, R.I., Arai, R., Waguri, S., Sato, M., Sato, K., Bar-Nun, S., Yoshimori, T., Noda, T., & Nagata, K.  
10 (2020). ERdj8 governs the size of autophagosomes during the formation process. *Journal of Cell Biology*,  
11 219(8), e201903127. <https://doi.org/10.1083/jcb.201903127>.  
12

13 Zhou, Y., Chen, Y., Xu, C., Zhang, H., & Lin, C. (2020). TLR4 Targeting as a Promising Therapeutic Strategy for  
14 Alzheimer Disease Treatment. *Frontiers in Neuroscience*, 14, 602508.  
15 <https://doi.org/10.3389/fnins.2020.602508>.  
16  
17  
18  
19  
20  
21  
22  
23  
24  
25  
26  
27  
28  
29  
30  
31  
32  
33  
34  
35  
36  
37  
38  
39  
40  
41  
42  
43  
44  
45  
46  
47  
48  
49  
50  
51  
52  
53  
54  
55  
56  
57  
58  
59  
60

For Peer Review

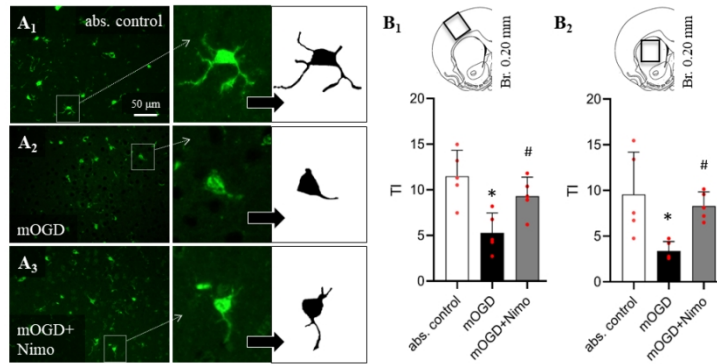


Figure 1. Quantitative analysis to evaluate the effect of nimodipine on microglial morphology in live brain slice preparations. A, Fluorescence immunohistochemistry images show Iba1-labeled microglia in absolute control brain slices (A<sub>1</sub>), in slices exposed to mild oxygen glucose deprivation (mOGD) (A<sub>2</sub>), and to mOGD in combination with nimodipine (mOGD+Nimo) (A<sub>3</sub>) in the cerebral cortex. Binary silhouettes of individual Iba1-positive microglia show the arborization of the cells. B, Transformation index (TI) calculated to quantify the degree of arborization (decreasing TI corresponds to an amoeboid shape and thus increasing activity) in the cortex (B<sub>1</sub>) and striatum (B<sub>2</sub>). Data were obtained as follows: The morphological phenotype of 15 microglia per brain slice were evaluated and the average was taken as a single data point. Five brain slices were analysed in each of the 3 experimental groups. Data are presented as mean±stdev (n=5/group). Normality of data distribution was determined by Shapiro-Wilk test (B<sub>1</sub>: p= 0.867; B<sub>2</sub>: p= 0.857). Data were analysed by one-way analysis of variance (ANOVA) (B<sub>1</sub>, f= 8.723, p=0.0046\*; B<sub>2</sub>, f= 6.501, p=0.0122\*) followed by Holm-Sidak's multiple comparisons test (p<0.05\* vs. abs. control; p<0.05# vs. mOGD).

338x190mm (96 x 96 DPI)

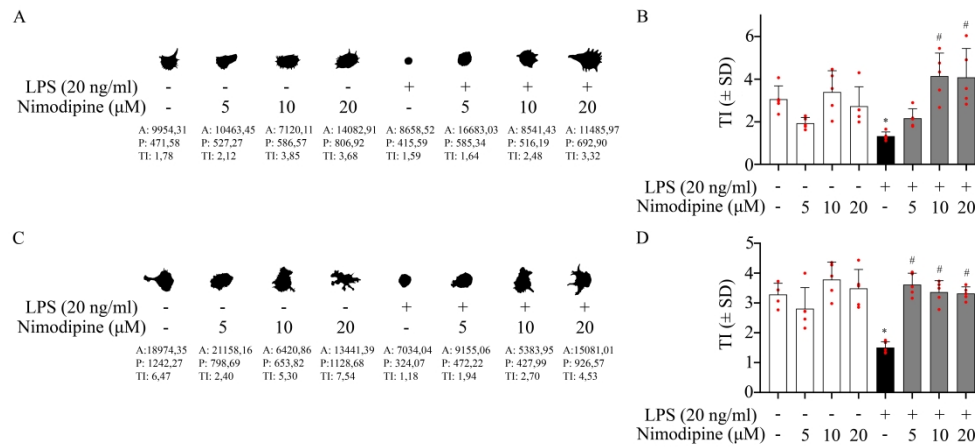


Figure 2. Quantitative analysis to evaluate the effect of nimodipine on microglial morphology in co-cultures (A-B) and microglia monocultures (C-D). A, Iba1-positive cell masks representative of microglia in co-cultures (DIV7). B, Microglial transformation index (TI) calculated for each experimental condition in co-cultures. C, Iba1-positive cell masks representative of microglia in mono-cultures (subDIV7). D, Transformation index (TI) calculated for each experimental condition in microglia mono-cultures. In A and C, the values are given below the masks: A, area; P, perimeter; TI, transformation index. In B and D, data were obtained as follows: The morphological phenotype of 15 randomly selected microglia per culture were evaluated and the average was taken as a single data point. Five cell cultures were analysed in each of the 8 experimental groups. Data are presented as mean $\pm$ stdev; red spheres represent individual values in each condition (n=15/experimental condition). Normality of the data distribution was determined by the Shapiro-Wilk test (B,  $p=0.340$ ; D,  $p=0.532$ ). Data were analysed by one-way analysis of variance (ANOVA) (B,  $f=7.419$ ,  $p<0.05^*$ ; D,  $f=11.880$ ,  $p<0.05^*$ ) followed by Tukey's multiple comparison ( $p<0.05^*$  vs. absolute control;  $p<0.05\#$  vs. LPS alone).

584x260mm (300 x 300 DPI)

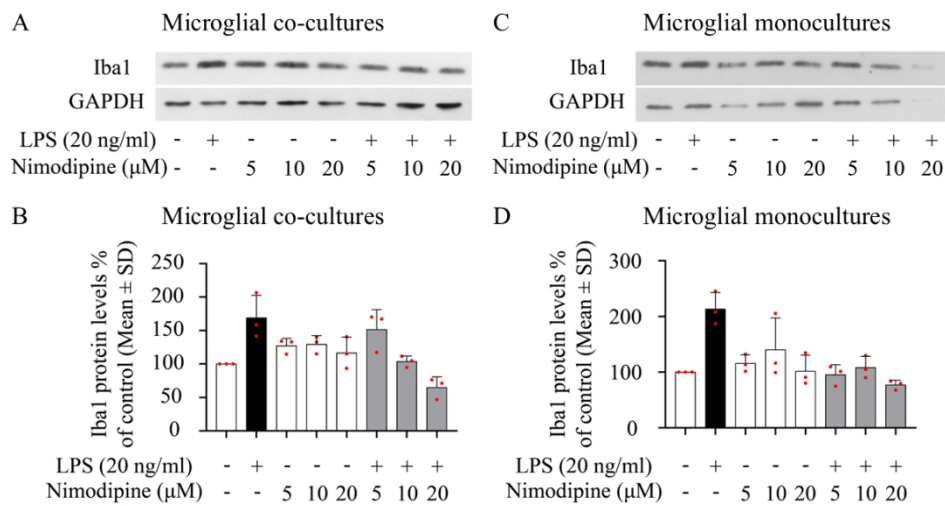
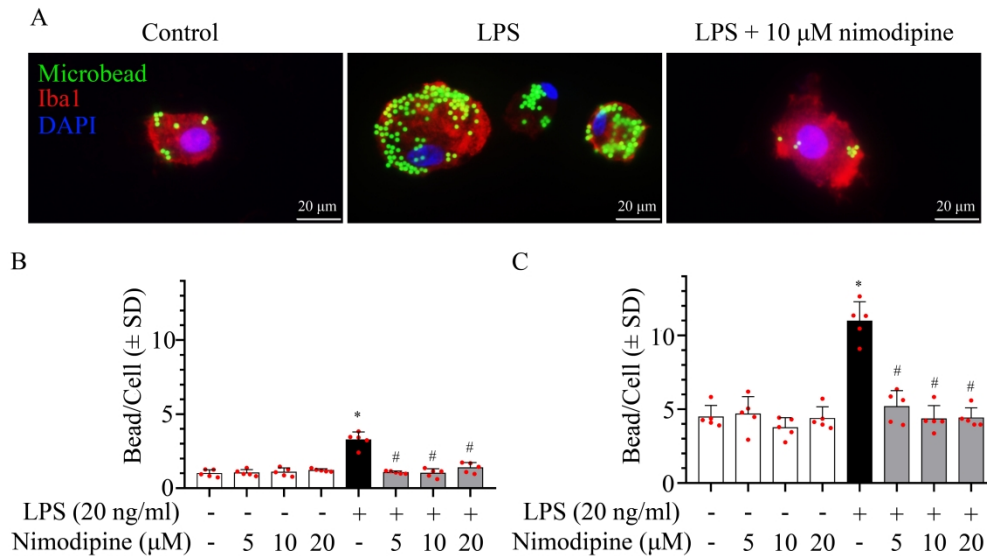


Figure 3. Exploratory quantitative analysis to detect the effect of nimodipine on microglial Iba1 protein levels in co-cultures (A-B) and microglial monocultures (C-D). A, Representative Western blot images for Iba1 and GAPDH, used as an internal control, obtained from co-cultures. B, Iba1 protein levels quantified in co-cultures. C, Representative Western blot images for Iba1 and GAPDH from microglial monocultures. D, Iba1 protein levels quantified in microglia monocultures. In A and C, images were scanned and processed with identical settings to allow comparisons between Western blots from different samples. In B and D, data are integrated optical density values relative to control, and the descriptive statistics present data as mean $\pm$ stdev. Red spheres indicate individual values (n=3) in each group.

338x190mm (96 x 96 DPI)



26  
27  
28  
29  
30  
31  
32  
33  
34  
35  
36

Figure 4. Evaluation of the effect of nimodipine on microglial phagocytic activity as visualized by fluorescent microbeads co-localized with Iba1 protein. A, Representative fluorescence microscopic images of Iba1-labeled microglia in monocultures. Fluorescent microbeads in their cytoplasm indicate increased phagocytic activity after LPS activation, which was counteracted by nimodipine. B, Phagocytotic activity of microglia quantified in co-cultures. C, Phagocytotic activity quantified in microglial monocultures. Note, that phagocytosis was typically seen in activated, amoeboid cells in all experimental groups. In B and C, data were obtained as follows: The morphological phenotype of 100 microglia per culture dish were evaluated and the average was taken as a single data point. Five cell cultures were analysed in each of the 8 experimental groups. Data are presented as mean $\pm$ stdev; red spheres represent individual cultures in each group. Normality of data distribution was determined by Shapiro-Wilk test (B,  $p=0.289$ ; C,  $p=0.264$ ). Data were analysed by one-way analysis of variance (ANOVA) (B,  $f=34.76$ ,  $p<0.05^*$ ; C,  $f=30.42$ ,  $p<0.05^*$ ) followed by Tukey's multiple comparison ( $p<0.05^*$  vs. absolute control;  $p<0.05\#$  vs. LPS alone).

37  
38  
39  
40  
41  
42  
43  
44  
45  
46  
47  
48  
49  
50  
51  
52  
53  
54  
55  
56  
57  
58  
59  
60

419x250mm (300 x 300 DPI)

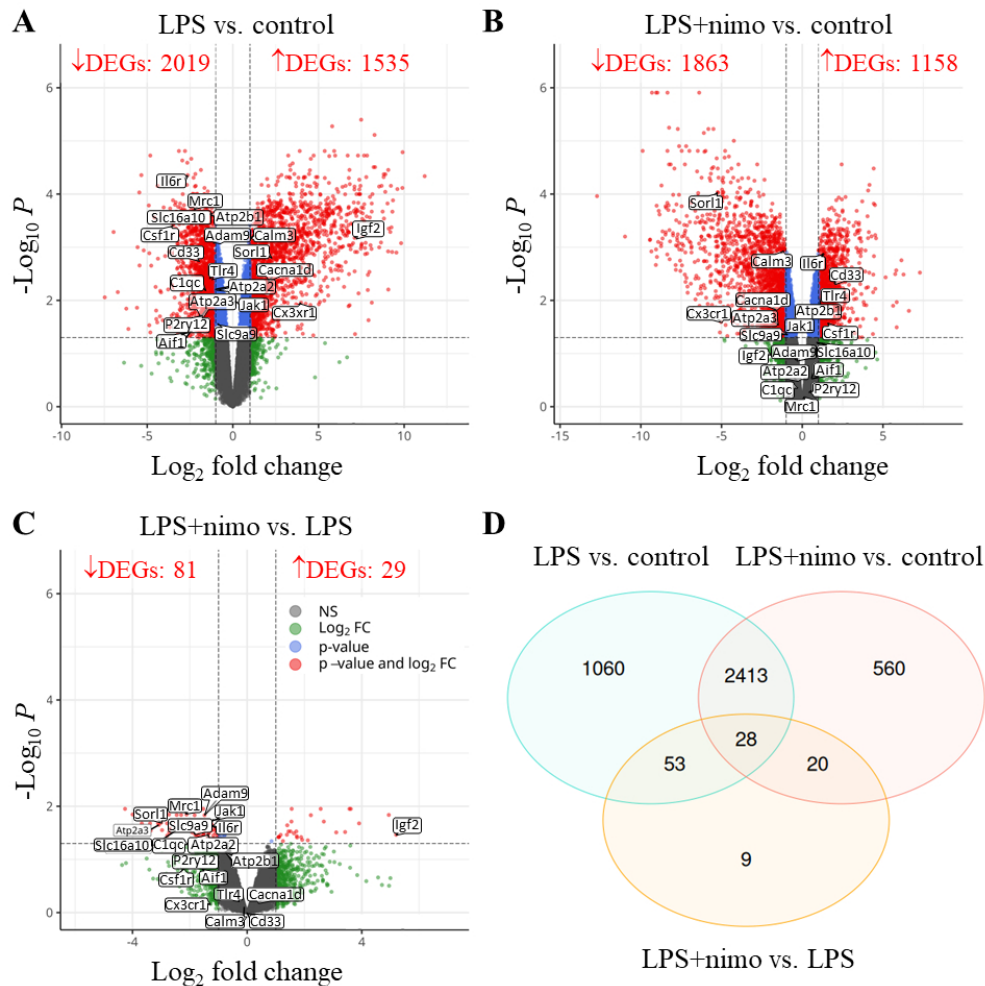


Figure 5. Activation with lipopolysaccharide (LPS) and treatment with nimodipine (nimo) cause alterations in rat primary microglia transcriptome. Volcano plots depict  $\log_2$  fold changes and  $\log_{10}$  of the adjusted p-value per gene comparing LPS vs. control (A), LPS+nimodipine treatment vs. control (B) and LPS+nimodipine treatment vs. LPS alone (C). Venn diagram shows the overlap of differentially expressed genes (DEGs) in the three experimental conditions (D). Cutoff values are  $\log_2\text{FC}=1$  and  $p=0.05$ .

254x260mm (96 x 96 DPI)

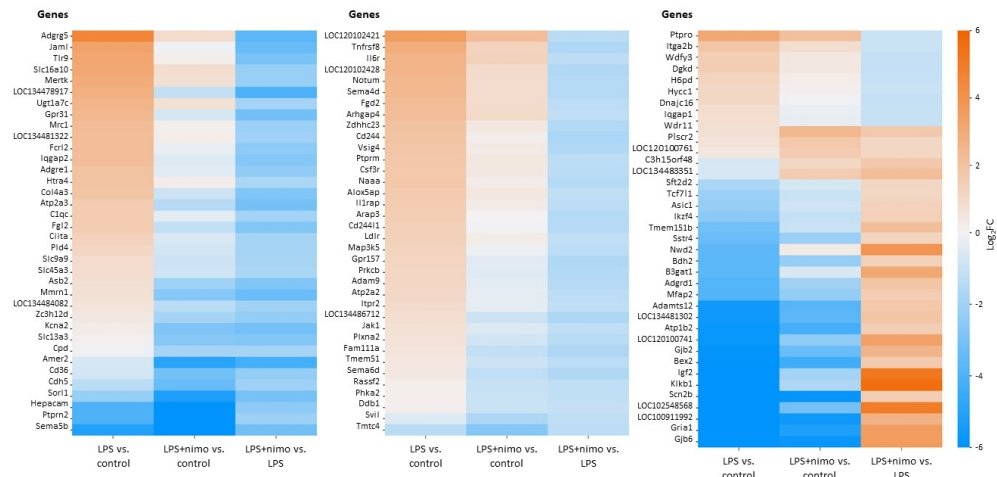


Figure 6. Heat maps of differentially expressed genes (DEGs) selected for significant change by nimodipine treatment (LPS+nimodipine) compared to LPS challenge alone (selection criteria:  $-1 > \text{Log}_2\text{FC} > 1$  and  $\text{adj.}p < 0.05$ ).

350x190mm (96 x 96 DPI)

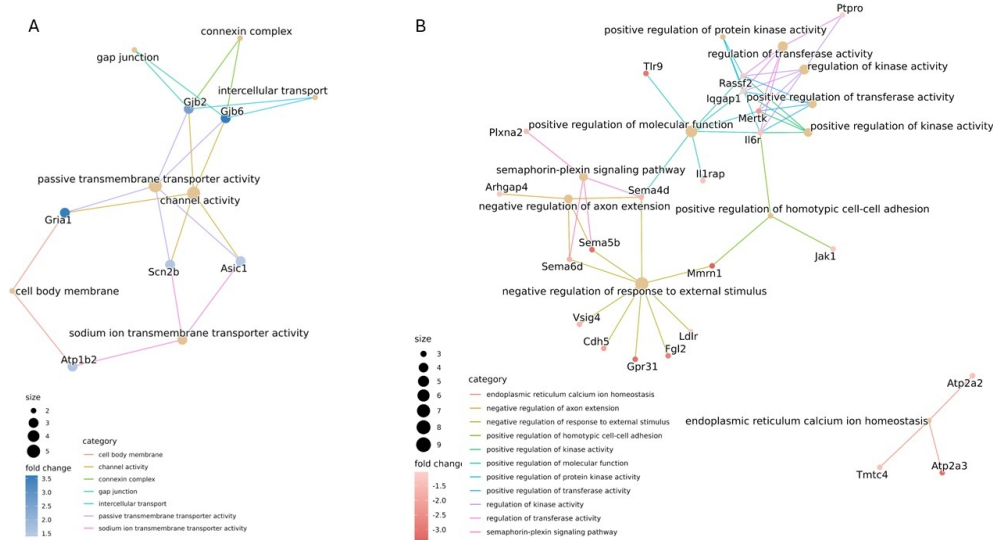


Figure 7. Functional enrichment analysis results are displayed in gene-concept network plots (cnet plots) to illustrate the effect of nimodipine on biological processes (BP). Upregulated (A) and downregulated (B) functions are shown by linkages of genes and gene ontology (GO) terms (LPS+nimodipine vs. LPS alone).

338x190mm (96 x 96 DPI)

		Gene	LPS vs. Control	LPS+nimo vs. Control
Voltage-gated channels	Cav2.1 (P/Q type)	<b>Cacna1a</b>	-0.7219*	-0.3948
	Cav2.2 (N type)	<b>Cacna1b</b>	0.6013	0.7139
	Cav1.2 (L type)	<b>Cacna1c</b>	-0.2578	0.3518
	Cav1.3 (L type)	<b>Cacna1d</b>	-2.0082*	-1.6291*
	Cav2.3 (R type)	<b>Cacna1e</b>	-6.3553*	-4.1933*
	Cav3.1 (T type)	<b>Cacna1g</b>	-1.3216*	-1.4446*
	Cav3.2(T type)	<b>Cacna1h</b>	-4.3333*	-3.1830*
	Ligand gated ion channels	NMDA glutamate receptor subunits	<b>Grina</b>	-0.3575
<b>Grin3a</b>			-5.7735*	-3.8086*
<b>Grin3b</b>			0.5822*	0.3713
<b>Grin2d</b>			-0.4088	-0.4464
AMPA glutamate receptor subunits		<b>Gria1</b>	-8.7561*	-5.1868*
		<b>Gria2</b>	-3.9386*	-7.4451*
		<b>Gria3</b>	0.4753	0.0275
Ionotropic purinergic receptors		<b>P2rx4</b>	1.1635*	0.4266
		<b>P2rx5</b>	1.6848	1.9936
		<b>P2rx7</b>	-0.5053	0.5582
TRP channel	TRPM2	<b>Trpm2</b>	1.8575*	0.9351
	TRPM7	<b>Trpm7</b>	-0.0819	-0.1983
	TRPV1	<b>Trpv1</b>	0.9004	0.8205
Calcium release-activated calcium channel		<b>Orai1</b>	0.2527	1.0148
Endoplasmic reticulum	Ryr	<b>Ryr2</b>	-3.9591	-4.6406*
		<b>Ryr3</b>	-2.4677*	-1.4115*
	Ip3R	<b>Itpr1</b>	-1.1016*	-1.3957*
		<b>Itpr2</b>	0.9807*	-0.2841
		<b>Itpr3</b>	-0.9831*	-1.2148*
	SERCA	<b>Atp2a2</b>	1.0718*	-0.2831
<b>Atp2a3</b>		1.5887*	-1.4889*	
Mito-chondrium	Mitochondrial Calcium Uniporter subunits	<b>Mcu</b>	-0.6424*	-0.4994*
		<b>Mcub</b>	-0.0008	0.4497
		<b>Mcur1</b>	0.0440	-0.4735
		<b>Slc8b1</b>	1.5158*	1.3136*
Calcium binding proteins	Iba1	<b>Aif1</b>	1.4998*	0.5662
		<b>Calm1</b>	-0.2130	0.4626
		<b>Calm2</b>	-0.4094	-0.3885
	Calmodulins	<b>Calm3</b>	-1.0347*	-1.1380*
		<b>Ppp3ca</b>	0.6170	0.6156
		<b>Ppp3cb</b>	-0.3496	-0.1691
	Calcineurin subunits	<b>Ppp3cc</b>	-0.6994*	-0.3446
		<b>Ppp3r1</b>	-0.1563	-0.0850
		<b>Rcan1</b>	-0.0053	-0.4070

Upregulated

Downregulated

	LPS+nimo vs. LPS
1	
2	
3	0.3272
4	0.1126
5	0.6097
6	0.3792
7	2.1620
8	-0.1231
9	1.1503
10	0.6107
11	1.9649
12	-0.2109
13	-0.0376
14	3.5692*
15	-3.5065
16	-0.4479
17	-0.7369
18	0.3088
19	1.0635
20	-0.9225
21	-0.1164
22	-0.0799
23	
24	0.7621
25	
26	-0.6815
27	1.0562
28	-0.2941
29	-1.2649*
30	-0.2317
31	-1.3549*
32	-3.0776*
33	0.1429
34	0.4505
35	-0.5175
36	-0.2022
37	-0.9336
38	0.6757
39	0.0209
40	-0.1033
41	-0.0014
42	0.1804
43	0.3549
44	0.0713
45	-0.4018
46	
47	
48	
49	
50	
51	
52	
53	No change
54	
55	
56	
57	
58	
59	
60	

For Peer Review

Function	Gene	Protein	LPS vs. Control	LPS+nimo vs. Control
Immune response	Tlr9	Toll Like Receptor 9	3.1561*	0.1871
	Il6r	Il6 receptor	2.6244*	1.3293*
	Fgd2	FGD2	2.2662*	0.9111*
	Tnfrsf8	TNF Receptor Superfamily Member 8 (CD30)	2.9473*	1.2885*
	Fcrl2	Fc Receptor Like 2	2.2251*	-0.2329
	Cd244	CD244	1.9378*	0.1964
	Vsig4	V-Set And Immunoglobulin Domain Containing 4	1.8700*	0.2840
	Csf3r	Colony Stimulating Factor 3 Receptor	1.7708*	0.3918
	Alox5ap	Arachidonate 5-Lipoxygenase Activating Protein	1.6148*	0.4358
	Il1rap	Interleukin 1 Receptor Accessory Protein	1.5784*	0.2614
	C1qc	Complement C1q C Chain	1.5763*	-0.3748
	Fgl2	Fibrinogen-like protein 2	1.5614*	-1.1598
	Cd244l1	CD244 molecule like 1	1.4525*	-0.0051
	Ciita	class II, major histocompatibility complex, transactivator	1.2981*	-0.5630
	Plid4	Phospholipase D Family Member 4	1.1346*	-0.7653*
	Jak1	Janus Kinase 1	0.6950*	-0.5573*
	Zc3h12d	Zinc Finger CCCH-Type Containing 12D	0.4047	-1.8988*
	Cd36	platelet glycoprotein 4	-0.7784	-1.7757*
Sstr4	Somatostatin Receptor 4	-3.3714*	-2.1223*	
Adams12	disintegrin and metalloproteinase with thrombospondin motifs 12	-5.5776*	-3.8356*	
Cell adhesion	Jaml	Junction Adhesion Molecule Like	3.3154*	-0.0721
	Itga2b	Integrin Subunit Alpha 2b	1.8737*	0.8655*
	Adam 9	ADAM Metallopeptidase Domain 9	1.1258*	-0.3609
	Cdh5	Cadherin 5	-1.3695*	-3.3867*
	Hepacam	Hepatic And Glial Cell Adhesion Molecule	-3.9963*	-6.4712*
	Gjb2	Gap Junction Protein Beta 2	-5.9060*	-3.3409*
	Gjb6	Gap Junction Protein Beta 6	-9.3566*	-5.7405*
Auto-phagy	Wdfy3	WD Repeat And FYVE Domain Containing 3	1.5122*	0.4130
	Dnajc16	DnaJ homolog subfamily C member 16	1.0805*	-0.0147

Upregulated

Downregulated

nimo+LPS vs. LPS	
1	-2.9690*
2	-1.2951*
3	-1.3551*
4	-1.6588*
5	-2.4579*
6	-1.7414*
7	-1.5861*
8	-1.3790*
9	-1.1789*
10	-1.1789*
11	-1.3169*
12	-1.9511*
13	-2.7212*
14	-1.4575*
15	-1.8612*
16	-1.8999*
17	-1.8999*
18	-1.2523*
19	-2.3034*
20	-2.3405*
21	-2.3405*
22	1.2491*
23	1.7420*
24	
25	-3.3875*
26	-1.0082*
27	-1.4866*
28	-2.0172*
29	-2.4749*
30	-2.4749*
31	2.5651*
32	3.6161*
33	
34	-1.0992*
35	-1.0952*
36	
37	
38	No change
39	
40	
41	
42	
43	
44	
45	
46	

For Peer Review

**SUPPLEMENTARY MATERIAL TO****Nimodipine reduces microglial activation in vitro as evidenced by morphological phenotype, phagocytic activity and high-throughput RNA sequencing**

István Pesti<sup>1,2</sup>, Valentin Varga<sup>3</sup>, Erda Qorri<sup>3</sup>, Rita Frank<sup>1,2</sup>, Diana Kata<sup>4</sup>, Krisztián Vinga<sup>2</sup>, Péter Archibald Szarvas<sup>1,2</sup>, Ákos Menyhárt<sup>1,2</sup>, Károly Gulya<sup>2</sup>, Ferenc Bari<sup>5</sup>, Eszter Farkas<sup>1,2</sup>

<sup>1</sup>Hungarian Centre of Excellence for Molecular Medicine – University of Szeged Cerebral Blood Flow and Metabolism Research Group, Szeged, Hungary; Somogyi u 4, 6720 Szeged, Hungary;

<sup>2</sup>Department of Cell Biology and Molecular Medicine, Albert Szent-Györgyi Medical School and Faculty of Science and Informatics, University of Szeged; Szeged, Hungary; Somogyi u 4, 6720 Szeged, Hungary

<sup>3</sup>Delta Bio 2000 Ltd., 6726 Szeged, Hungary

<sup>4</sup>Institute of Laboratory Medicine, University of Szeged, Szeged, Hungary

<sup>5</sup>Department of Medical Physics and Informatics, Albert Szent-Györgyi Medical School and Faculty of Science and Informatics, University of Szeged; Szeged, Hungary; Korányi fasor 9, 6720 Szeged, Hungary

**\*Correspondence**

Eszter Farkas, D.Sc. (ORCID: 0000-0002-8478-9664)

HCEMM-USZ Cerebral Blood Flow and Metabolism Research Group

Department of Cell Biology and Molecular Medicine

Szent-Györgyi Albert Medical School

Faculty of Science and Informatics

University of Szeged

Somogyi u. 4

H-6720 Szeged

Hungary

Tel.: +36 62 342 208

E-mail: [farkas.eszter.1@med.u-szeged.hu](mailto:farkas.eszter.1@med.u-szeged.hu)

**Table S1.** Primary and secondary antibodies used for immunocytochemistry and Western blotting

Method	Model	Primary antibody	Company	Final dilution	Secondary antibody	Company	Final dilution
Immuno-cytochemistry	Cell culture	Rabbit anti-Iba1 polyclonal	Abcam, Cambridge, England	1:1000	Alexa Fluor 568 goat anti-rabbit	Invitrogen, Carlsbad, CA, USA	1:1000
	Brain slice preparation	Rabbit anti-Iba1 polyclonal	Abcam, Cambridge, England	1:300	Alexa Fluor™ 488 goat anti-rabbit	Thermo Fisher Scientific, USA	1:1000
Western blot	Cell culture	Rabbit anti-Iba1 polyclonal	Abcam, Cambridge, England	1:1000	Anti-rabbit IgG, peroxidase conjugated	Sigma, St. Louis, MO, USA	1:1000
		Mouse anti-GAPDH monoclonal	Sigma, St. Louis, USA	1:20000	Anti-mouse IgG, peroxidase conjug.	Sigma, St. Louis, MO, USA	1:1000

**Table S2.** Splice variants of the Cacna1c and Cacna1d transcripts.

Event type description	Genes					
	Cacna1c			Cacna1d		
	LPS vs. control	LPS+nimo vs. control	LPS+nim. vs. LPS	LPS vs. control	LPS+nimo vs. control	LPS+nim. vs. LPS
<b>Skipped exon</b>	11	14	14	9	9	9
<b>Alternative 5' splice sites</b>	1	1	1	0	0	0
<b>Alternative 3' splice sites</b>	0	0	0	2	2	2
<b>Mutually exclusive exons</b>	5	7	7	4	4	4
<b>Retained intron</b>	0	0	0	0	0	0

rMATS was utilized for the identification of potential splice variants. The following sample comparisons were run with rMATS: (i) Control vs LPS, (ii) Control vs LPS-Nimo, and (iii) LPS vs LPS-Nimo. The FASTQ files for each sample group along with the GTF file were used as input for rMATS and the parameters with the exception of readLength (set to 151) were kept unchanged. With rMATS the following splicing events were identified: (i) skipped exons, (ii) alternative 5' splice site, (iii) alternative 3' splice site, and (iv) mutually exclusive exons.

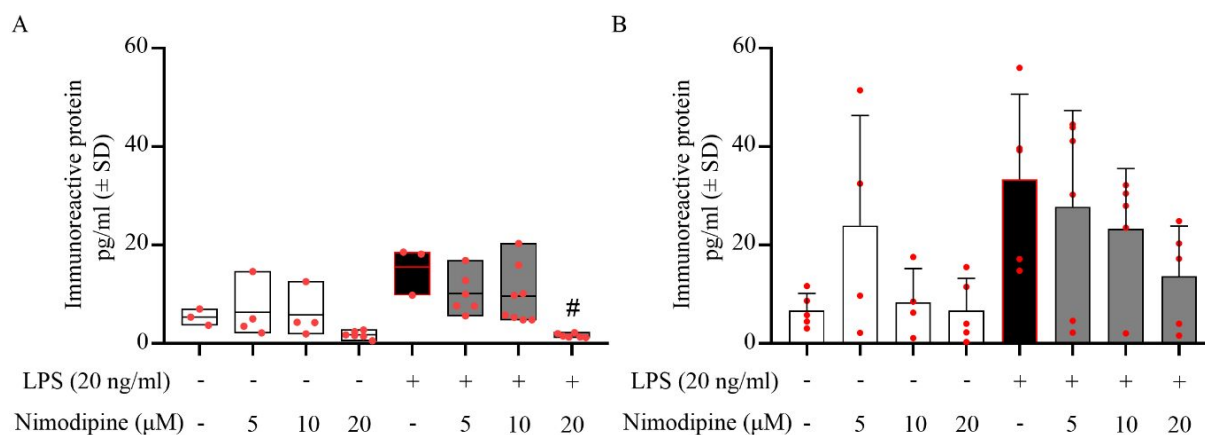


**Figure S1.** The effect of nimodipine on microglial tumor necrosis factor- $\alpha$  secretion (TNF- $\alpha$ ). **A**, Quantitative analysis of TNF- $\alpha$  concentration in the cell culture medium of co-cultures by ELISA. **B**, Quantitative analysis of TNF- $\alpha$  levels in the monoculture medium by ELISA. Data are presented as mean $\pm$ SD; red spheres represent individual values in each group. Normality of data distribution was determined by Shapiro-Wilk test (A,  $p=0.025$ ; B,  $p=0.175$ ). Data were analysed by Kruskal-Wallis test ( $p<0.05^*$ ) followed by Dunn's multiple comparison ( $p<0.05^{\#}$  vs. LPS alone) (A) or one-way analysis of variance (ANOVA) ( $f=2.783$ ,  $p=0.0229^*$ ) followed by Tukey's multiple comparison (B).

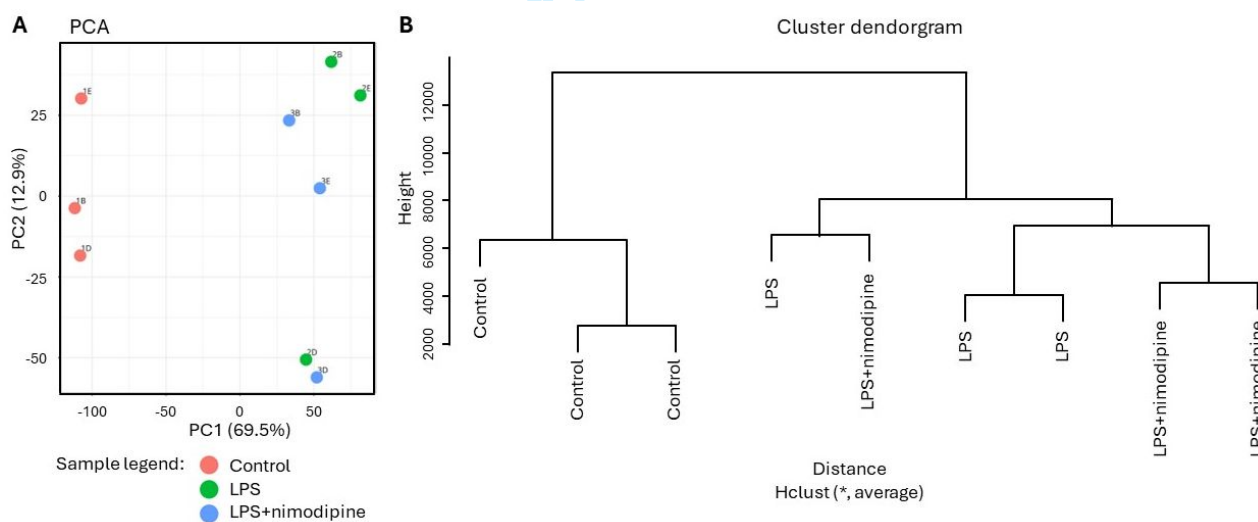
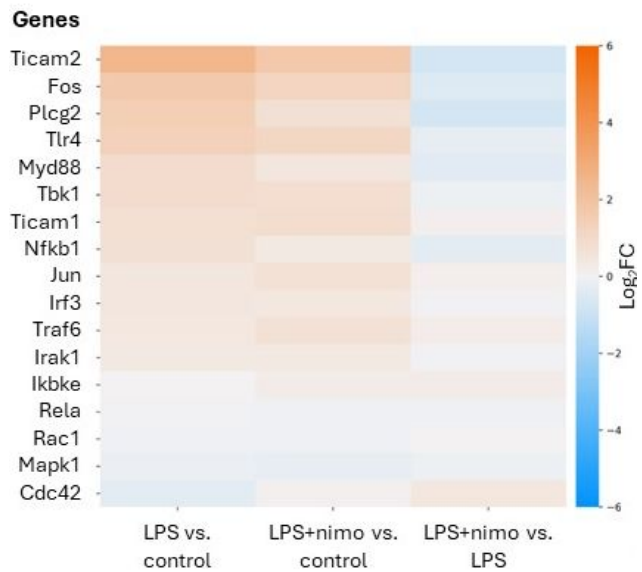
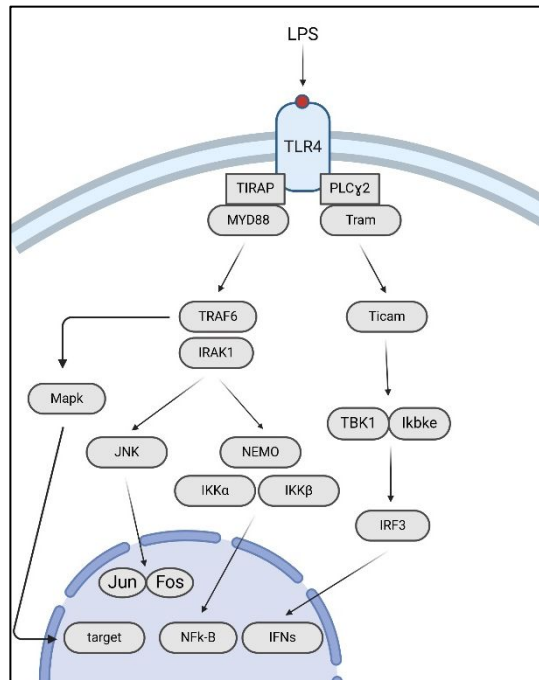


**Figure S2.** Principal component analysis (PCA) (A) and hierarchical clustering of the three replicate samples in each of the three experimental conditions.



	Gene	Protein	LPS vs. Control	LPS+nimo vs. Control	LPS+nimo vs. LPS
Log <sub>2</sub> FC Myd88 - NF-κβ pathway	<b>Tlr4</b>	Toll-like receptor 4	1.37631551515627**	1.09774830548889*	-0.27856720966738
	<b>Myd88</b>	Myeloid differentiation factor 88	0.931297115866776*	0.512311231834087	-0.418985884032688
	<b>Irak1</b>	Interleukin-1 receptor-associated kinase 1	0.357718285600152*	0.328923346021234	-0.0287949395789173
	<b>Traf6</b>	Tumor necrosis factor receptor associated factor 6	0.467529170810678	0.696125210666336*	0.228596039855658
	<b>Mapk1</b>	Mitogen-activated protein kinase 1	-0.144796783427549	-0.244740745151777	-0.0999439617242279
	<b>Nfkb1</b>	Transcription factor p50	0.706608116226361	0.346044877459237	-0.360563238767124
	<b>Rela</b>	Transcription factor p65	-0.0212808455524724	-0.0701113902856001	-0.0488305447331276
	<b>Jun</b>	AP-1: JUN-FOS heterodimer	0.494667025286904	0.657971280634847	0.163304255347943
	<b>Fos</b>	AP-1: JUN-FOS heterodimer	1.7043808354236**	1.19247391804049**	-0.511906917383109
Log <sub>2</sub> FC PLCγ2 - INF pathway	<b>Plcg2</b>	Phospholipase C γ2 (PLCγ2)	1.45833426933459**	0.731765024424296	-0.726569244910291
	<b>Ticam1</b>	TIR domain containing adaptor molecule 1	0.775816919399679*	0.874848554650933*	0.0990316352512544
	<b>Ticam2</b>	TIR Domain Containing Adaptor Molecule 2	2.50271525074297***	1.77603141407565**	-0.726683836667323
	<b>Tbk1</b>	TANK-binding kinase 1	0.911893805852649**	0.798928253826634**	-0.112965552026014
	<b>Ikbke</b>	IkB kinase ε (IKKε)	0.0047473690303157	0.254485048445809	0.249737679415493
	<b>Irf3</b>	IFN regulatory factor 3 (IRF3)	0.478015475906282	0.431368854662145	-0.0466466212441361

Change in mRNA expression is expressed as Log<sub>2</sub>FC (adjusted p<0.001\*\*\*, p<0.01\*\*, p<0.05\*); Cells showing data Log<sub>2</sub>FC>1 and adjusted p<0.05\* are color-coded.



**Figure S3.** Graphical illustration, heat map and table of Log<sub>2</sub>FC values of differentially expressed genes (DEGs) of the TLR4 intracellular signaling cascades. The illustration was created in Biorender.

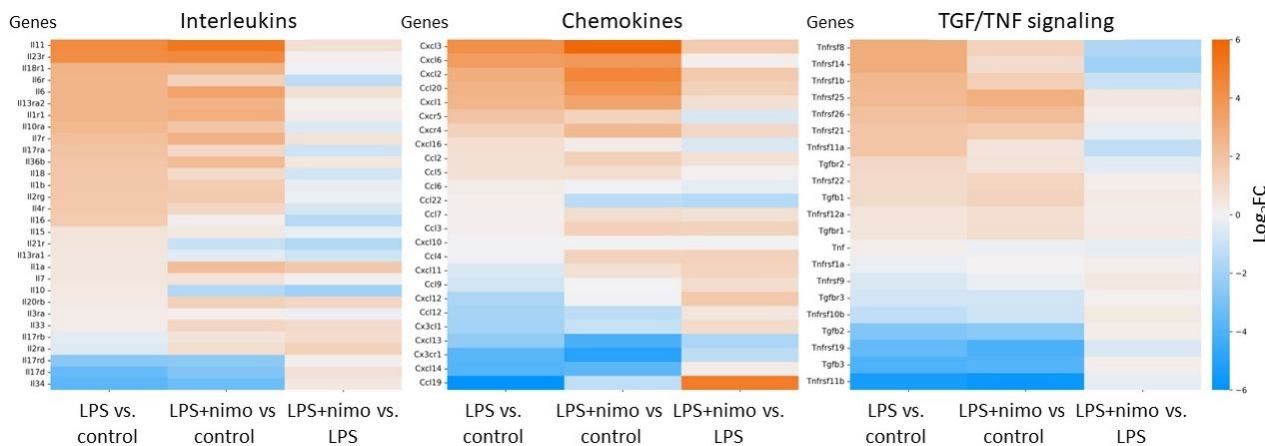
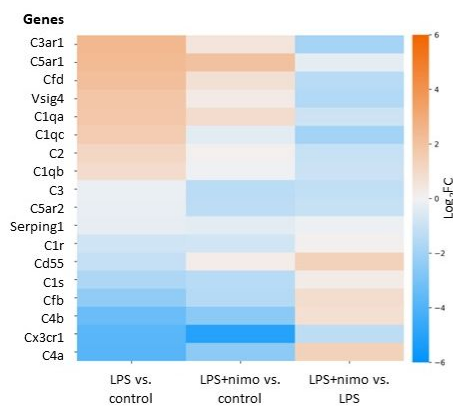
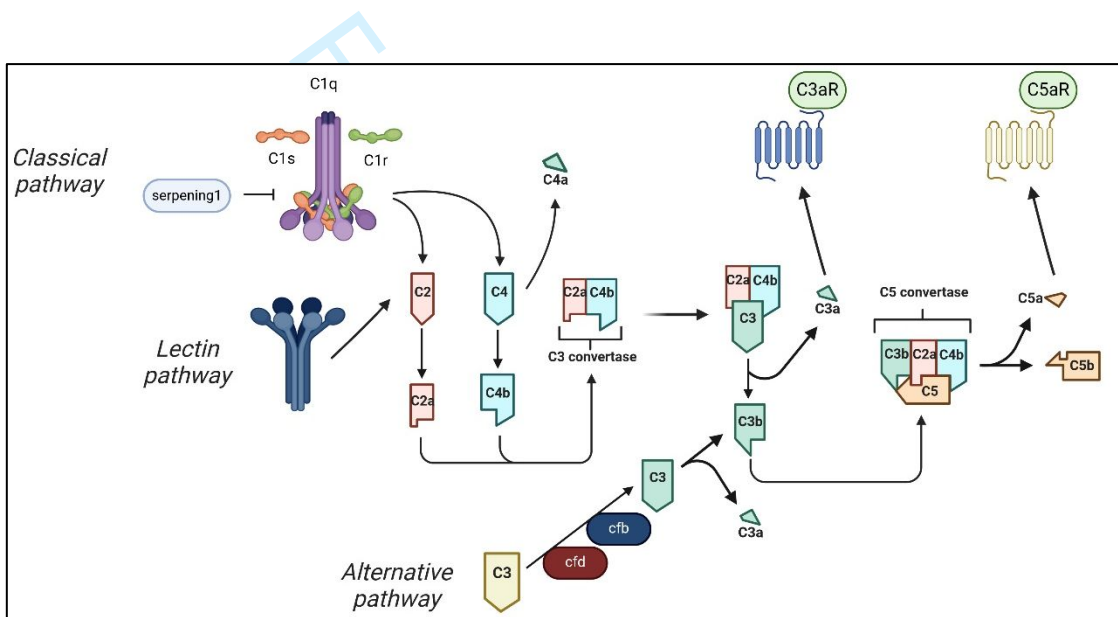


**Figure S4.** Heat maps of differentially expressed genes (DEGs) of cytokine production and cytokine receptors.

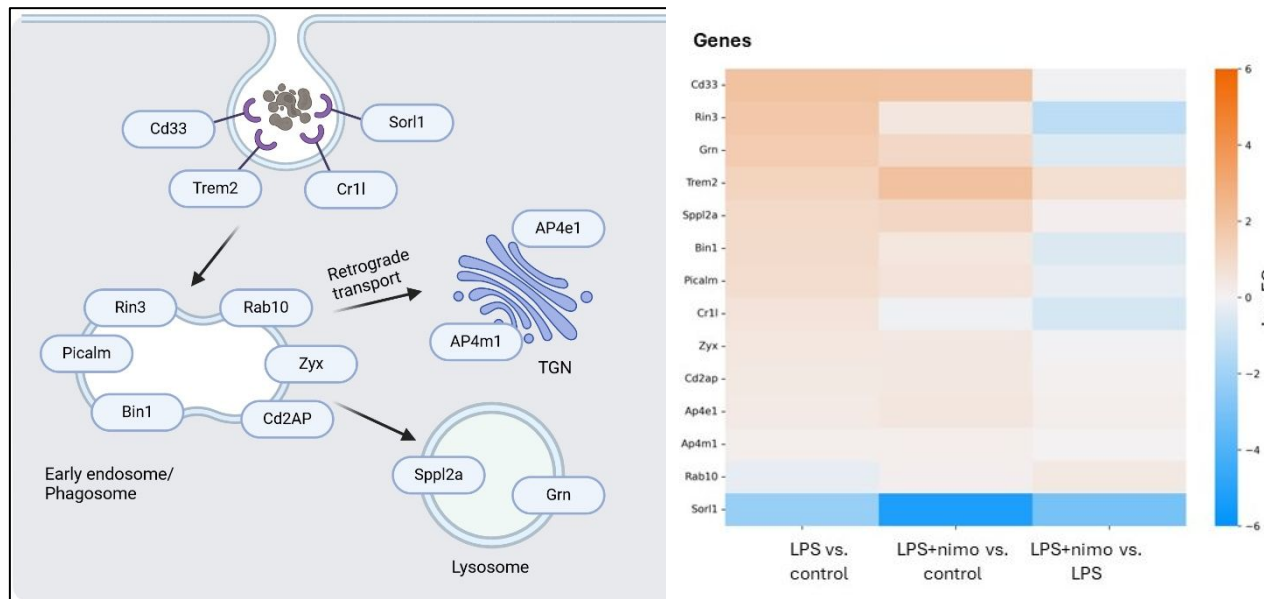


Gene	Protein	LPS vs. Control	LPS+nimo vs. Control	LPS+nimo vs. LPS
<b>C1qa</b>	Complement C1q A Chain	1.82433043708043***	0.928424065985502*	-0.895906371094926
<b>C1qb</b>	Complement C1q B Chain	0.896139078483293*	-0.062506611460651	-0.958645689943944
<b>C1qc</b>	Complement C1q C Chain	1.57631055227281**	-0.374787907205631	-1.95109845947844*
<b>C1r</b>	Complement C1r	-0.850703878735754*	-0.792384791981425*	0.0583190867543291
<b>C1s</b>	Complement C1s	-1.70735508510492**	-1.4385904449904**	0.26876464011452
<b>C2</b>	Complement C2	1.16186560967228	0.0842001954108209	-1.07766541426146
<b>C3</b>	Complement component 3	-0.164554619452472	-1.36932715797576*	-1.20477253852328
<b>C3a1</b>	Complement C3a receptor 1	2.41299902712663**	0.516743386236297	-1.89625564089033
<b>C4a</b>	Complement component C4A	-3.84310089396165***	-2.5049664110849**	1.33813448287675
<b>C4b</b>	Complement component C4b	-3.34420140892777**	-2.57181261248509*	0.772388796442677
<b>C5a1</b>	Complement C5a receptor 1	2.31960851870402***	2.01720129811001**	-0.302407220594009
<b>C5a2</b>	Complement C5a receptor 2	-0.227071521505924	-1.29550332563333**	-1.06843180412741

Change in mRNA expression is expressed as Log2FC (adjusted p<0.001\*\*\*, p<0.01\*\*, p<0.05\*); Cells showing data Log2FC>1 and adjusted p<0.05\* are color-coded.

Upregulated Downregulated No change

**Figure S5.** Graphical illustration of the complement cascade, and heat map and table of Log<sub>2</sub>FC values of differentially expressed genes (DEGs) of the complement cascade. The table represents elements of the classical pathway. The illustration was created in Biorender.



Gene	Protein	LPS vs. Control	LPS+nimo vs. Control	LPS+nimo vs. LPS
Mertk	MER proto-oncogene, tyrosine kinase	2.954339485***	0.745642691*	-2.208696794*
Trem1	Triggering receptor expressed on myeloid cells 1	2.65946549*	2.089265562*	-0.570199928
Cd14	CD14	2.554088221*	2.914597914*	0.360509693
Ms4a4a	Membrane spanning 4-domains A4A	2.465338006**	1.20453917	-1.260798836386
Pilra	Paired immunoglobulin like type 2 receptor alpha	2.294493209**	1.732118696**	-0.562374512
Itgb3	Integrin subunit beta 3	2.024810148**	1.330887784*	-0.693922364
Cd33	CD33	1.97489407177189**	1.9584104421259**	-0.0164836296459843
Itgam	Integrin subunit alpha M	1.935057939***	0.707422549	-1.22763539
P2ry12	Purinergic receptor P2Y12	1.834086719*	0.396802193	-1.437284526
Msr1	Macrophage scavenger receptor 1	1.658905523*	1.506334711*	-0.152570812
Cd68	CD68	1.626088502*	1.986906668**	0.360818166
Ms4a6a	Membrane spanning 4-domains A6A	1.484376764*	1.194112931	-0.290263833
Scarb2	Scavenger receptor class B member 2	1.247925926*	0.671130929	-0.576794997
Tyrobp	Transmembrane immune signaling adaptor TYROBP	1.1908533*	1.27844057*	0.08758727
Itgav	Integrin subunit alpha V	1.133289596*	-0.171504758	-1.304794354
Clec7a	C-type lectin domain containing 7A	1.408250927	2.003534565*	0.595283638
Trem2	Triggering receptor expressed on myeloid cells 2	1.24708943709988	2.03656841920013*	0.789478982100245
Scarb1	Scavenger receptor class B member 1	0.796881174	0.930924298	0.134043123
Axl	AXL receptor tyrosine kinase	0.410712113	0.230587349	-0.180124764
Olr1	Oxidized low density lipoprotein receptor 1	-0.57346171	1.220056852	1.793518562
Cd36	CD36	-0.778365124	-3.118829281**	-2.340464158*
Tyro3	TYRO3 protein tyrosine kinase	-1.194974178**	-1.377515693**	-0.182541515
Sorl1	Sortilin-related receptor	-2.23557087074647**	-5.23766018660087***	-3.0020893158544*

Change in mRNA expression is expressed as Log<sub>2</sub>FC (adjusted p<0.001\*\*\*, p<0.01\*\*, p<0.05\*); Cells showing data Log<sub>2</sub>FC>1 and adjusted p<0.05\* are color-coded.



**Figure S6.** Graphical illustration, heat map and table of Log<sub>2</sub>FC values of differentially expressed genes (DEGs) of markers of phagocytosis. The illustration was created in Biorender.

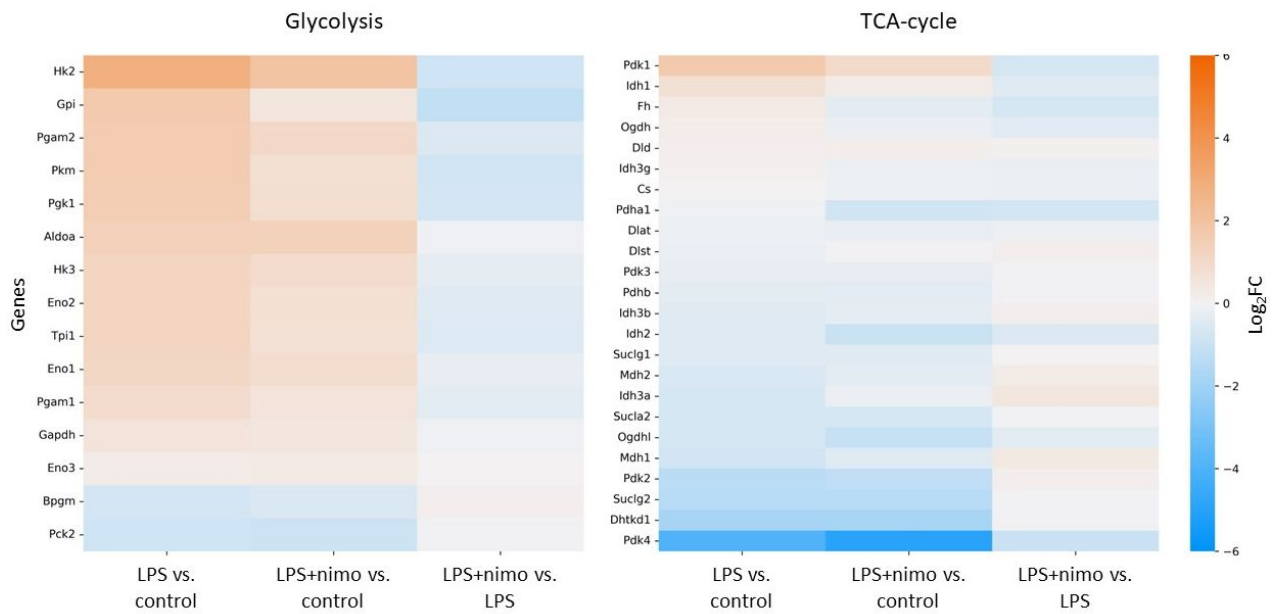


**Figure S7.** Heat map of differentially expressed genes (DEGs) of glycolysis and the mitochondrial tricarboxylic acid (TCA) cycle.

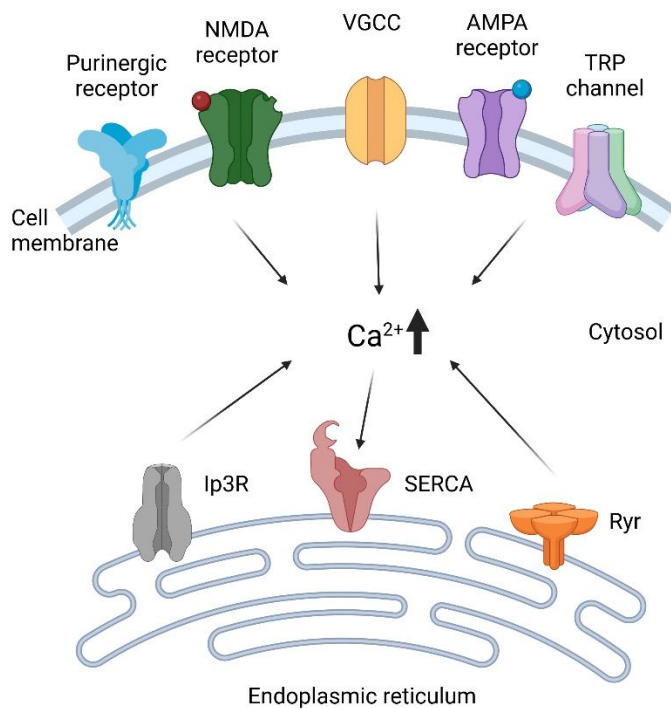


**Figure S8.** Molecular pathways of cytosolic Ca<sup>2+</sup> accumulation and Ca<sup>2+</sup> removal in microglia. The illustration was created in Biorender.

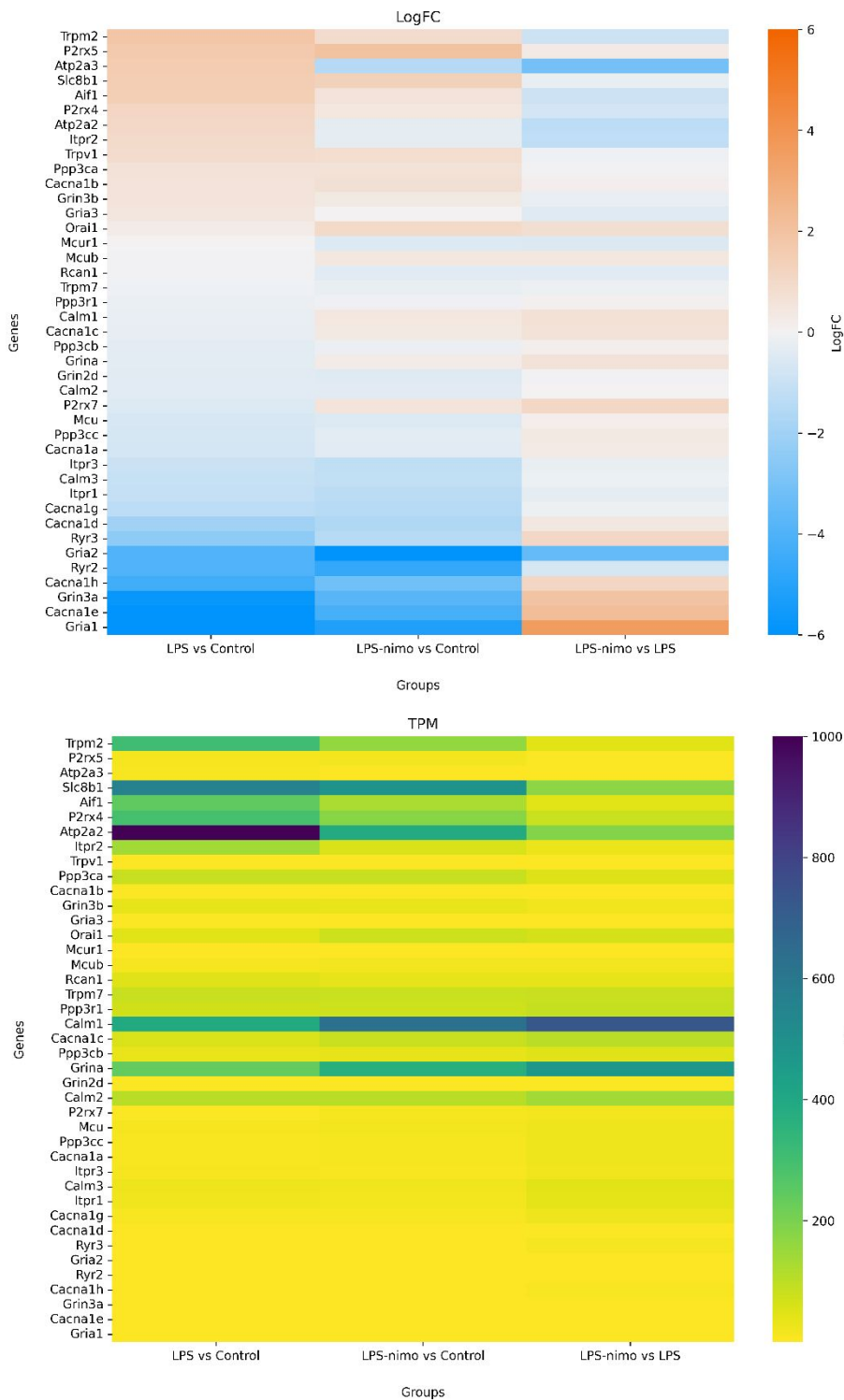


**Figure S9.** Log<sub>2</sub>FC and TPM colour scale heatmaps complementing Table 1 showing changes in gene expression of calcium channels and calcium binding proteins in primary microglia monoculture.

